THE Journal OF THE AMERICAN LEATHER CHEMISTS ASSOCIATION

September 2023 Vol. CXVIII, No.9 *JALCA* 118(9), 357–400, 2023

118th Annual Convention

May 21–23, 2024
Hershey Lodge
325 University Drive
Hershey, PA 17033

For more information go to:
leatherchemists.org/
annual_convention.asp

Contents

Distributed by
University of CINCINNATI
LIBRARY PUBLISHING SERVICES

An imprint of the University of Cincinnati Press

ISSN: 0002-9726

Communications for Journal Publication

Manuscripts, Technical Notes and Trade News Releases should contact:
Mr. Steven D. Lange, Journal Editor, c/o University of Cincinnati, 5997 Center Hill Ave., Bldg. C, Cincinnati, OH 45224, USA
E-mail: jalcaeditor@gmail.com Mobile phone: (814) 414-5689

Contributors should consult the Journal Publication Policy at:
http://www.leatherchemists.org/journal_publication_policy.asp

SPONSORS FOR THE 117th ANNUAL MEETING

ADMIRAL —$4,500

North American Minerals Corporation

ELITE —$4,000

TFL USA/Canada, Inc.

PLATINUM — $3,500

Erretre SpA
Stahl USA

DIAMOND —$2,500

Buckman
Pangea Made, Inc.

GOLD LEVEL — $1,750

American Chrome & Chemicals LTP Inc.
Dow Coating Materials
Tannin Corporation

SILVER LEVEL — $1500

Atlas Refinery Inc.
D. R. Diedrich and Co.
Hermann Oak Leather Co.
JBS USA
NTE Company (Pty) Ltd
Quaker Color
Tyson Foods, Inc.

BRONZE LEVEL — $1000

Chemtan Company
Cromogenia Units
Curfimex SA de CV
Leather Miracles
SB Foot Co./Red Wing Shoe Co.
Twin City Hides
Union Specialties Inc.
Wickett & Craig of America

JOURNAL OF THE
AMERICAN LEATHER CHEMISTS ASSOCIATION

Proceedings, Reports, Notices, and News
of the
AMERICAN LEATHER CHEMISTS ASSOCIATION

THE JOURNAL OF THE AMERICAN LEATHER CHEMISTS ASSOCIATION (USPS #019-334) is published monthly by The American Leather Chemists Association, c/o University of Cincinnati, 5997 Center Hill Ave., Bldg. C, Cincinnati, Ohio 45224. Telephone (513) 290-2505. Single copy price: $10.00 members, $20.00 non-member plus shipping and handling. Subscriptions: $185 for hard copy plus postage and handling of $60 for domestic subscribers and $70 for foreign subscribers; $220 for ezine only; and $240 for hard copy and ezine plus postage and handling of $60 for domestic subscribers and $70 for foreign subscribers.

Periodical Postage paid at Cincinnati, Ohio and additional mailing offices. Postmaster send change of addresses to The American Leather Chemists Association, c/o University of Cincinnati, 5997 Center Hill Ave., Bldg. C, Cincinnati, Ohio 45224.

Website: www.leatherchemists.org E-mail: hallks@ucmail.uc.edu

COLD
Milling

Smooth Leather Milling

Erretre
Tannery Innovations

Erretre s.p.a. | Via Ferraretta,1 | Arzignano (VI) 36071 | tel. +39 0444 478312 | info@erretre.com

Fluorescent Tracing of Dialdehyde Sodium Alginate Tanning Agent in Leather Matrix

by
Min Zhu,[1] Yudan Yi,[1] Jia Fu,[1] Yunhang Zeng[1] and Ya-nan Wang[1,2,*]
[1]*National Engineering Laboratory for Clean Technology of Leather Manufacture,*
Sichuan University, Chengdu 610065, China
[2]*Key Laboratory of Leather Chemistry and Engineering of Ministry of Education,*
Sichuan University, Chengdu 610065, China

Abstract

Dialdehyde polysaccharides possess a sustainable nature and good tanning performance. However, the lack of specific detectable groups in their molecular structure results in the difficulty in the determination of the location of dialdehyde polysaccharides in leather fiber networks. In this study, dialdehyde sodium alginate (DSA) tanning agent was fluorescent labeled by 5-(4,6-dichlorotriazinyl) aminofluorescein (DTAF). The purified DTAF–DSA showed high and stable fluorescent intensity at emission wavelength of 515.2 nm when the pH was over 6.0, and the temperature was in the range of 20°C to 50°C. DTAF–DSA was used in tanning and tracked using fluorescence microscopy. Its penetration in the fiber network could be clearly visualized, and its distribution in leather differed with the molecular weight of DSA. As a result, this fluorescence tracing technique could display the mass transfer behavior of dialdehyde polysaccharide tanning agents in leather matrix, which will provide underlying data for tanning mechanism exploration.

Introduction

Tanning is the most essential process of leather-making to convert raw hide/skin into durable leather. Currently, the development of chrome-free tanning technologies to replace chrome tannage is in full swing[1-3] because of the potential environmental risk of hexavalent chromium.[4-6] In particular, a trend toward biomass-based chrome-free tanning system is emerging in recent years to support a more sustainable leather industry.[7-9] Polysaccharides and their derivatives, such as cellulose[10-12] starch[13-16] and alginate,[17-19] have been modified to produce biomass-based tanning agents. Among them, dialdehyde polysaccharides produced by periodate oxidation is regarded as a promising tanning agent due to its high reactivity and adjustable molecular size.[19-20] Degradation of polysaccharides via glycosidic bond breaking co-occurs with aldehyde group formation in periodate oxidation. However, the reported dialdehyde polysaccharide tanning agents exhibited molecular weights of in the thousands,[11,16,18] much higher than traditional tanning agents. This raised questions whether the dialdehyde polysaccharide tanning agent can penetrate the hierarchical hide/skin matrix and carry out tanning effectively. Unlike mineral tanning agents, the organic dialdehyde polysaccharide cannot be distinguished with collagen matrix by using EDS analysis.[21] Therefore, it is necessary to establish a method to monitor the penetration (mass transfer behavior) and distribution of dialdehyde polysaccharide tanning agent in leather, which in turn explores the effect of mass transfer on the tanning performance.

Fluorescent tracing technique can visually trace and display the distribution of leather chemicals in leather matrix. It has been applied in the location of enzymes,[22-24] acrylic resin retanning agents,[25-27] amino resin retanning agents[28,29] and fatliquors.[30-32] The brief procedure for this technique is described below. Fluorescein was used to label these chemicals via covalent binding at first. Then the fluorescent labeled chemical was introduced into skin/leather under the conventional conditions. Fluorescence microscopic techniques were used for the observation of skin/leather sections to achieve the location of the chemical within collagen fibers. Our previous work reported that aldehyde tanning agents could be visualized through the autofluorescence of Schiff base formed by aldehyde and amino groups of collagen. However, this approach was not sensitive enough to detect dialdehyde polysaccharides.[33] Fluorescent labeling may be more suitable for this type of tanning agent.

In this study, dialdehyde sodium alginate (DSA) was chosen as the model object of dialdehyde polysaccharide tanning agent due to its satisfactory tanning effects.[18,34] Considering that hydroxyl groups are the most common functional groups of polysaccharides, fluorescent labeling with the hydroxyl of DSA was performed in order to establish a universal method. Then the penetration and distribution of the fluorescent labeled DSAs with different molecular weights in the tanned leather was visualized using fluorescence microscopy to verify if this is an effective approach to characterize the mass transfer behavior of dialdehyde polysaccharide tanning agent.

*Corresponding author email: wangyanan@scu.edu.cn
Manuscript received March 5, 2023, accepted for publication April 8, 2023.

Experimental

Materials

Sodium alginate (SA), sodium periodate, ethanediol and ethanol were of analytical grade and purchased from Chengdu Kelong Chemical Co., Ltd (Chengdu, China). 5-(4,6-dichlorotriazinyl) aminofluorescein (DTAF) was purchased from Aladdin Biochemical Technology Co., Ltd (Shanghai, China). Sephadex G-25 was purchased from Sigma-Aldrich Co. LLC. All the chemicals used for the analyses were of analytical grade, and the chemicals used for leather processing were of commercial grade.

Preparation of DSA

DSA was prepared according to Ding's method.[18] Sodium periodate (17.28 g) was dissolved in 500 mL ultrapure water, and then 20.0 g SA was added during stirring. After stirring for 24 h in the dark, the reaction was terminated by 4.5 mL ethanediol for 0.5 h. The product solution was fractionated by ethanol precipitation as follows. Firstly, 55.56 mL ethanol was added to obtain 10% ethanol-water solution (v/v). After standing at 4°C for 72 h, the solution was filtered by vacuum filtration. Then, the filtrate was precipitated using 20% ethanol-water solution (v/v) by adding extra 69.45 mL ethanol at 4°C for 72 h. The precipitate was separated and purified by dialysis with ultrapure water as the dialysis medium (dialysis bag MWCO 300 Da), and the retentate was lyophilized into DSA with high molecular weight (H–DSA). The filtrate was precipitated using 35% ethanol-water solution (v/v) by adding extra 144.23 mL ethanol at 4°C for 72 h. DSA with moderate molecular weight (M–DSA) was obtained by separation and purification in the same way as above. In addition, 500 mL ethanol was added into the initial product solution at 4°C for 72 h. The precipitate was separated and purified by dialysis as well. The retentate was lyophilized into DSA with low molecular weight (L–DSA).

Fourier Transform Infrared (FT-IR) spectroscopy analysis

SA or DSA was mixed with potassium bromide powder and pressed into a tablet. Then the FT-IR spectra of SA and DSA were determined using a FT-IR spectrometer (Nicolet Is50, Thermo Fisher, USA). The wavenumber ranged from 500 to 4000 cm^{-1}. The resolution was 4 cm^{-1}, and the cumulative number of scans was 32.

Determination of aldehyde group content of DSA

The aldehyde group content of DSA was determined by hydroxylamine hydrochloride titration method.[35] In brief, freeze–dried DSA (0.1000 g) was dissolved in 25 mL ultrapure water. The pH value of the DSA solution was adjusted to 5.0 with HCl/NaOH solution. The pH of 20 mL hydroxylamine hydrochloride solution (0.25 mol/L) was adjusted to 5.0 with NaOH solution. The above two solutions were mixed evenly and reacted at 40°C for 4 h in a water bath shaker. Then, the pH of the mixture was titrated to 5.0 with 0.1 mol/L NaOH solution, and the volume of titrant was recorded to calculate the aldehyde group content of DSA.

Preparation of DTAF labeled DSA (DTAF–DSA)

DSAs with different molecular weights were labeled according to the method of Abitbol T et al. with some modifications.[36] Dichlorotriazine, the reactive group of DTAF, can covalently bind with hydroxyl of DSA. DSA (0.5 g) was reacted with 7.5 mg DTAF in 12.5 mL borax-NaOH buffer (pH 9.5) in the dark with stirring for 24 h. The product was concentrated with PEG-20000 to a final volume of 4 mL, filtered through 0.45 μm filter units, and then loaded onto a Sephadex G-25 gel-filtration column (1.6 cm × 50 cm) to remove unreacted DTAF. Borax/boric acid buffer (pH 9.0) was used as the mobile phase with a flow rate of 0.06 mL/min. The eluate fractions (3 mL/tube) were collected automatically, and the absorbance of each fraction was measured at 490 nm (the absorbance maximum of DTAF) using an UV–Vis spectrophotometer (UV–1899PC, Mapada, China). The DTFA–DSA fractions without DTAF were collected. Borax/boric acid were removed from the collected fractions via dialysis in ultrapure water (dialysis bag MWCO 300 Da) until the pH of dialysate reached 7.0. The retentate was lyophilized into DTAF–DSA.

Analysis of fluorescence emission spectra

Fluorescence emission spectra of DTAF (20 mg/L), DSA (100 mg/L), DTAF–H–DSA (100 mg/L), DTAF–M–DSA (100 mg/L) and DTAF–L–DSA (100 mg/L) were measured by fluorescence spectrophotometer (F–7100, Hitachi, Japan) with 492 nm excitation wavelength of (the excitation maximum of DTAF). Fluorescence emission was recorded from 500 to 620 nm.

Thermal and pH stability of DTAF–DSA

The temperature of DTAF–L–DSA solutions (100 mg/L) were held at 20°C, 25°C, 30°C, 35°C, 40°C, 45°C and 50°C, respectively, for 20 min. Then the fluorescence emission spectra of the solutions were determined with 492 nm excitation wavelength to evaluate the thermal stability of DTAF–DSA.

The pH values of DTAF–L–DSA solutions (100mg/L) were adjusted to 3.00, 4.00, 5.12, 6.17, 6.96, 8.05 and 8.96 with HCl/NaOH solution and held at room temperature for 1 h. Fluorescence emission spectra of these solutions were determined with an excitation wavelength of 492 nm to evaluate the pH stability of DTAF–DSA.

Determination of molecular weight

The size exclusion chromatography (SEC, 1260 Infinity II, Agilent, USA) was used to measure the weight average molecular mass (M_w) and polydispersity (PDI) of DSA and DTAF–DSA. The sample solution (5 mg/mL) was filtered through 0.45 μm filter units and then analyzed under the following conditions. The injection volume was 50 μL. A TSK-gel GMPWXL column (7.8 mm × 300 mm, Tosoh, Japan) was equipped. $NaNO_3$ solution (0.1 mol/L) was used as the mobile phase at a flow rate of 0.6 mL/min.[37] The column temperature was maintained at 30°C. Pullulan standards from 180 Da to 600 kDa (Agilent, UK) were used for calibration.[38] The results were processed with OmniSEC 4.7 software.

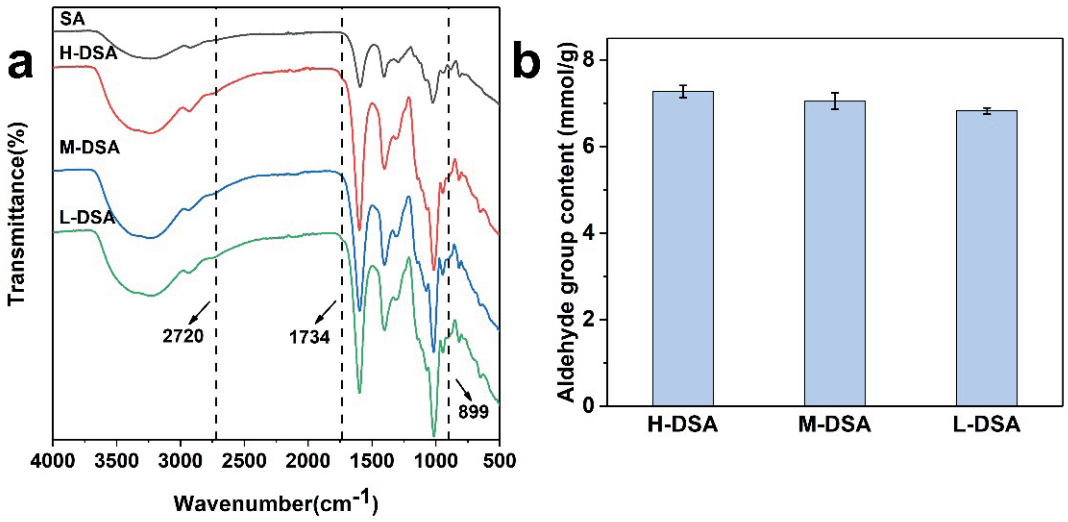

Figure 1. FT–IR spectra of SA and DSAs **(a)** and aldehyde group content of DSAs **(b)**

Observation of DTAF–DSA during tanning

Several pieces of pickled cattle hide (1.5 g each, from symmetrical parts of butt along the backbone) were rewetted and depickled to pH 7.0 with sodium bicarbonate. Then they were divided into eighteen groups (two pieces in each group) for the following tanning trials. DTAF–DSAs with different molecular weights were used as the tanning agents. Every six groups were tanned with 4% of one type of tanning agent (a mixture of DTAF–DSA and DSA with the mass ratio of 1:4) and 100% water (based on limed weight) at 25°C for 15 min, 45 min, 1 h, 2 h, 2.5 h and 4 h, respectively. After tanning, the samples were cut into vertical sections (thickness, 20 μm) using a freezing microtome (CM1950, Lecia, Germany). Sections were observed via an inverted fluorescence microscope (DMi8, Lecia, Germany) to locate DTAF–DSA in the leather. The relative content of DTAF–DSA in the leather was analyzed from the micrograph by Image J software.[39] Furthermore, the sections were stained with hematoxylin and eosin (HE). The bright field photographs of HE stained sections were obtained by an inverted fluorescence microscope (DMi8, Lecia, Germany) to show the collagen fiber structure.

Results and Discussion

Characteristics of DSA

FT–IR analysis and aldehyde group content determination were performed to verify if aldehyde groups were formed on DSA after periodate oxidation of SA. Compared with the infrared spectrum of SA, the infrared spectrum of DSAs showed new absorption peaks of aldehyde carbonyl group at 899 cm^{-1} (stretching vibration of hemiacetal), 1734 cm^{-1} (C=O stretching vibration of aldehyde group) and 2720 cm^{-1} (C–H stretching vibration of aldehyde group)[40-42] (Figure 1a). Moreover, DSAs with different molecular weights exhibited similar aldehyde group content of 6.8–7.3 mmol/g (Figure 1b). These results indicated that aldehyde groups were successfully introduced into DSA.

Characteristics of DTAF–DSA

Typical functional groups of DSA, including hydroxyl (–OH), carboxyl (–COOH), and aldehyde group (–CHO) were available for fluorescence labeling. Dichlorotriazine, the reactive group of DTAF, has strong reactivity with hydroxyl of DSA through a nucleophilic substitution reaction in alkaline conditions (pH > 9) at room temperature.[43] Thus, DSA could be labeled by DTAF (see Figure 2).

Purification is needed to remove the excessive DTAF because the unreacted fluorescein residues will interfere with the tracing of DTAF–DSA in leather. Column chromatography was conducted using a Sephadex G-25 gel-filtration column to remove the unreacted DTAF (Figure 3). The reaction mixtures were separated into different fractions, and the main component in relatively high purity was collected as DTAF–DSA.

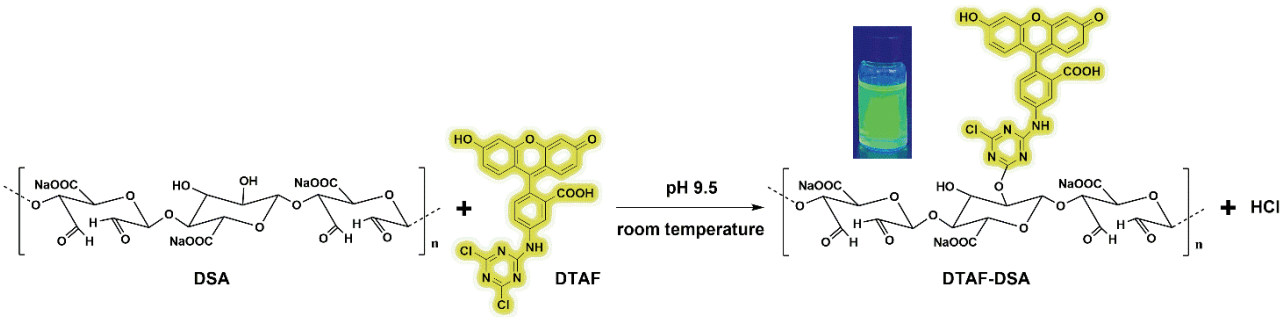

Figure 2. Schematic diagram of the DTAF labeling reaction with DSA.

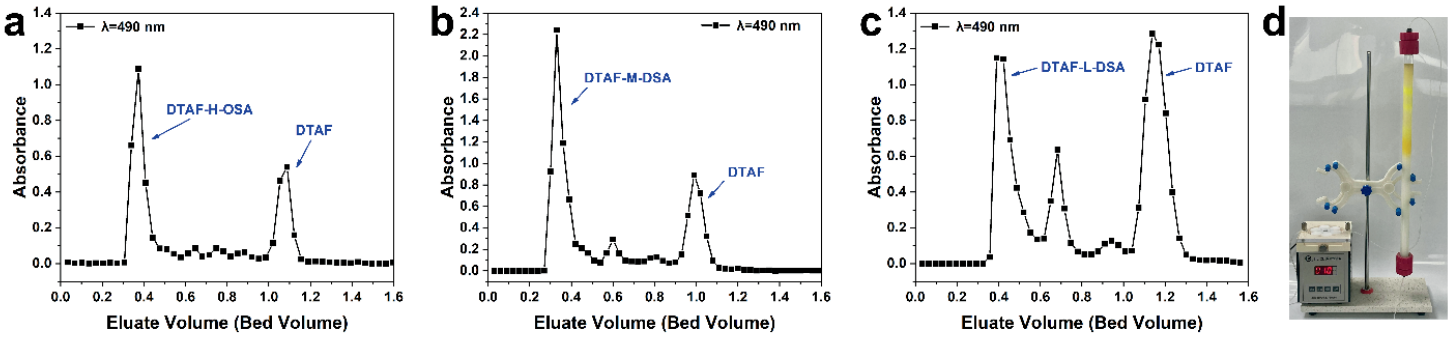

Figure 3. Chromatogram of **(a)** DTAF–H–DSA, **(b)** DTAF–M–DSA and **(c)** DTAF–L–DSA on **(d)** Sephadex G-25 gel-filtration column (1.6 cm × 50 cm). The column was eluted with borax/boric acid buffer (pH 9.0) at a rate of 0.06 mL/min.

The molecular weight of a tanning agent has a significant influence on its mass transfer and distribution in leather fiber network.[19] The molecular weights of DSA and DTAF–DSA with different sizes were determined before and after labeling. The molecular weights of the unlabeled DSAs showed a gradual decline because of the ethanol fractional precipitation (Table I). The molecular weights of DSAs decreased after labeling by DTAF. The most probable reason is DSA degradation in the alkaline labeling conditions (pH 9.5, 24 h). Another possible cause is the loss of unlabeled components in DSA during column chromatography. Even so, the DTAF labeled DSAs exhibited molecular weight gradients from approx. 25000 to 10000, which favored the investigation of the effect of DSA molecular weight on the mass transfer of the tanning agent in leather. The PDI of DSAs meant that DSAs had relatively narrow distribution. PDI of a tanning agent will influence its mass transfer in leather. In our previous work,[18] DSA with wide molecular weight distribution (high PDI) could endow leather with satisfactory comprehensive properties. Hence, an effective approach to characterize the mass transfer behavior of dialdehyde polysaccharide tanning agent could explore the effect of mass transfer on the tanning performance and help design PDAs with better tanning effect which have more suitable molecular weight and PDI.

The fluorescence spectra of DTAF, unlabeled DSA and purified DTAF–DSA were recorded at excitation wavelength of 492 nm (Figure 4). DTAF and DTAF–DSA exhibited the maximum emission at 515.2 nm, while unlabeled DSA showed absence of fluorescence. This result indicated that DTAF could successfully graft on DSA and give DSA detectable fluorescence to realize the visualization of mass transfer of DSA in leather fiber network.

The effects of pH and temperature on the fluorescent intensity of DTAF–DSA were explored to verify if the fluorescent DSA is visualized under the tanning conditions. As shown in Figures 5(a)

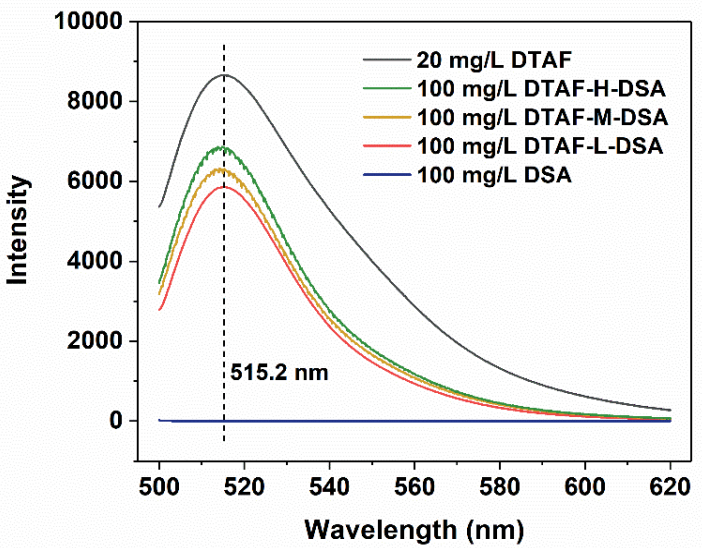

Figure 4. Fluorescence emission spectra of DTAF (20 mg/L), DTAF–H–DSA (100 mg/L), DTAF–M–DSA (100 mg/L), DTAF–L–DSA (100 mg/L) and DSA (100 mg/L) obtained using excitation wavelength of 492 nm (the excitation maximum of DTAF)

Table I

Molecular weight of DSA and DTAF–DSA

	M_w	PDI		M_w	PDI
H–DSA	77834	2.87	DTAF–H–DSA	24653	3.90
M–DSA	54972	2.50	DTAF–M–DSA	17241	3.60
L–DSA	26200	1.64	DTAF–L–DSA	9842	1.82

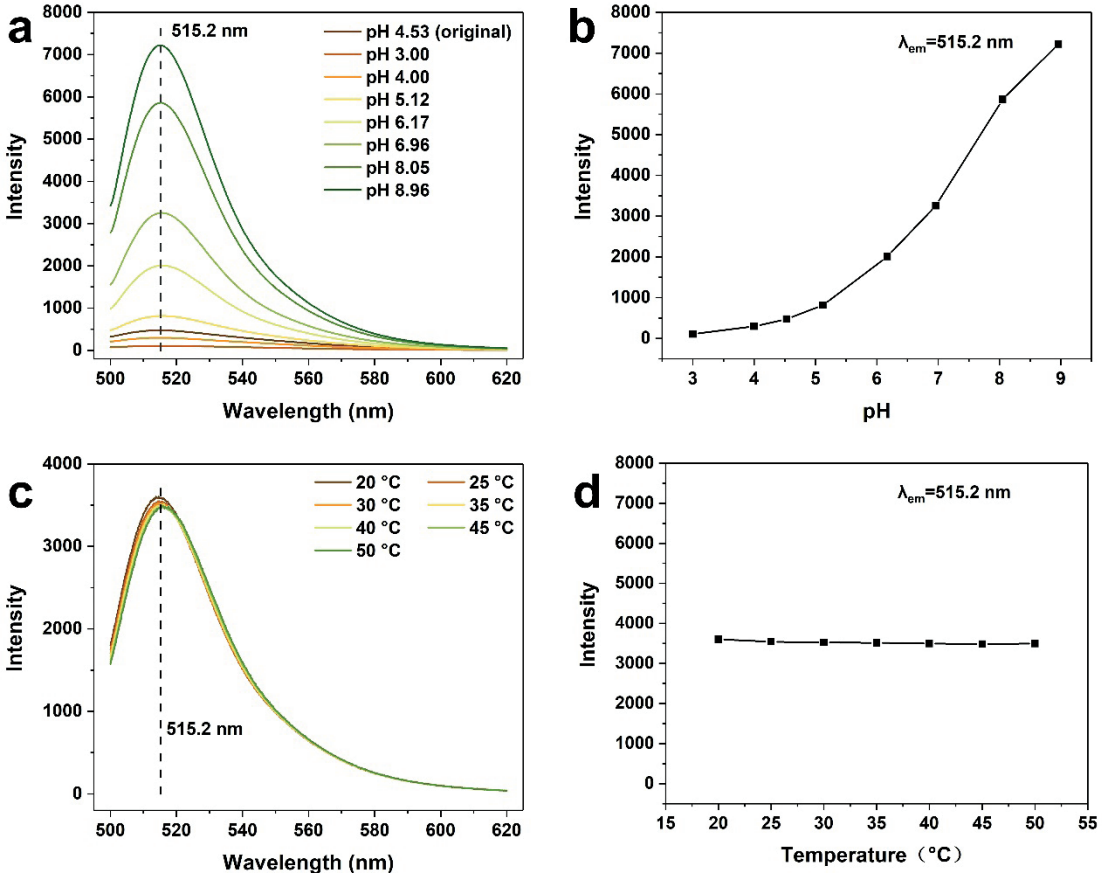

Figure 5. Fluorescence emission spectra of DTAF–L–DSA at different pH values **(a)** and temperatures **(c)**. Effects of pH **(b)** and temperature **(d)** on the fluorescent intensity of DTAF–L–DSA at emission wavelength of 515.2 nm. The excitation wavelength was 492 nm

and 5(b), the fluorescent intensity of DTAF–DSA is sensitive to pH changes. The intensity increased significantly as the pH value rose from 3 to 9. Thus, the recommended application pH value for DTAF–DSA was higher than 6.0. The isoelectric point of pickled hide is around 5.5~6.0.[44-45] When the pH is higher than 6.0, the pickled hide is negatively charged, which favors the penetration of DSA (rich in carboxyl groups, also negatively charged over pH 6.0) into leather. Considering the aldehyde tanning mechanism and previous experience of DSA tanning,[17,18] pickled hide was depickled to pH 7.0 before tanning to ensure the fluorescent tracing of DTAF–DSA during tanning. The penetration and distribution of DSA is expected to be accurately observed under this condition. As shown in Figures 5(c) and 5(d), there was little change in the fluorescence intensity of DTAF–DSA in the temperature range of 20°C to 50°C. Hence, 25°C was chosen for fluorescent tracing of DTAF–DSA as well as tanning.

Fluorescent tracing of DTAF–DSA in Leather

Pickled hide was depickled to pH 7.0 and then tanned by a mixture of DSA and DTAF–DSA at 25°C. The trace of DTAF–DSA in the leather fiber network was observed using a fluorescence microscope at different time points. The cross-sections of leather are shown in Figure 6. Collagen fibers in pickled hide were stained red with HE, and DTFA–DSA (green) were visible within collagen fiber network from the fluorescence micrographs. Image J software quantitatively analyzed the relative content of DTAF–DSA from Figure 6 and clearly showed the distribution of DSA in the leather (see Figure 7). The rewetted and depickled hides as control exhibited no detectable fluorescence because fluorescent labeled DSA was not added before tanning. Fluorescence appeared in both grain and flesh sides in the initial period of tanning, while no fluorescence was observed in the middle layer of hide. This result indicated that DSA started to permeate from the grain and flesh layers. The fluorescence brightness of the middle layer gradually increased with tanning time, which illuminated that DSA transferred to the core of the hide from grain and flesh. After a period of tanning, the fluorescence brightness along the cross-section was uniform and reached a plateau as shown in Figure 7. The phenomenon suggested that DSA fully penetrated in collagen fiber network.

DSAs with varying molecular weights were applied in tanning and exhibited different mass transfer characteristics. DTAF–H–DSA (M_w 24653) fully penetrated and evenly distributed in the cross-section of leather after 120 min. The penetration durations for DHAF–M–DSA (M_w 17241) and DTAF–L–DSA (M_w 9842) were shortened to 105 min and 60 min, respectively. These results suggested that the molecular weight of DSA tanning agent played a critical role in the penetration rate of DSA. The penetration rate increased with decreasing molecular weight of DSA. This regularity

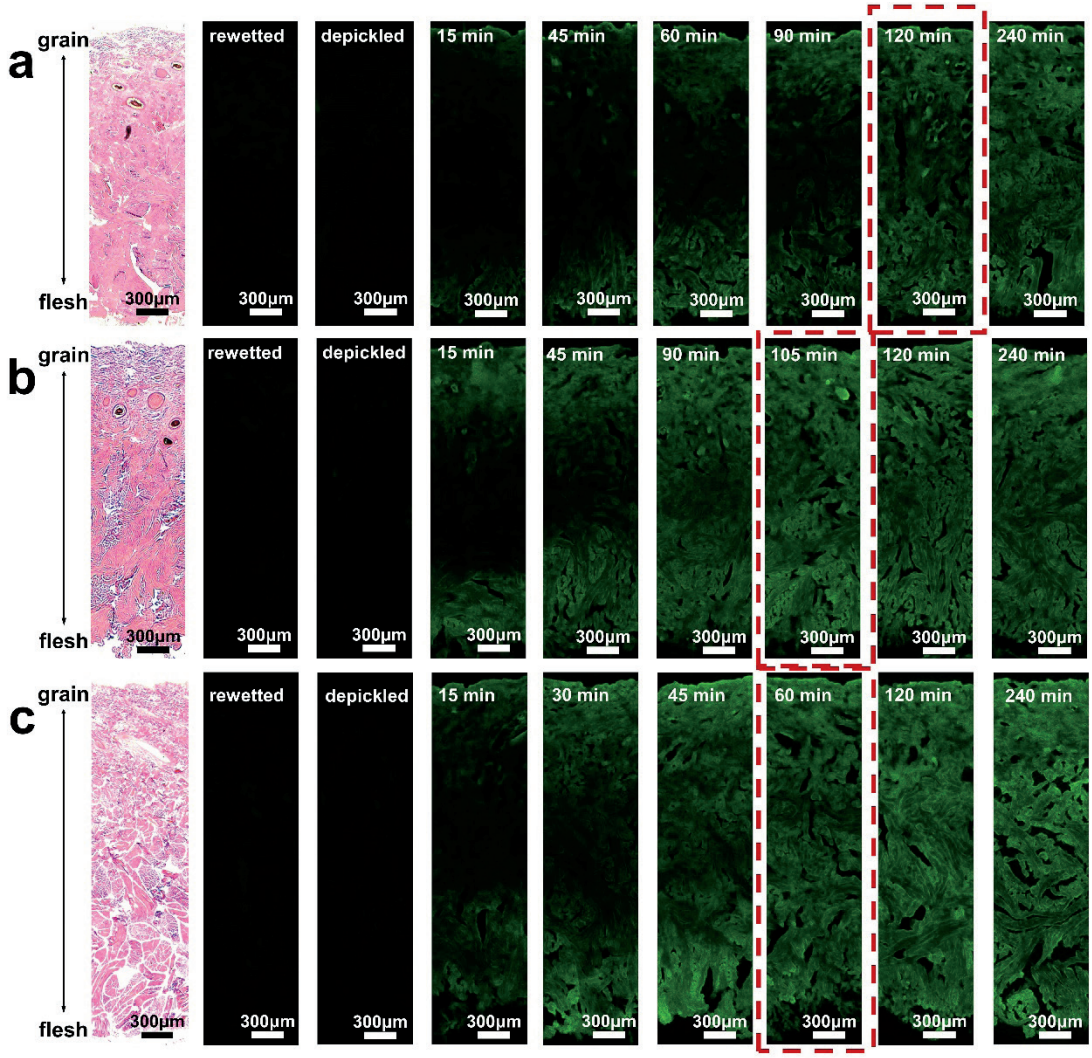

Figure 6. HE–stained bright field micrographs and fluorescence micrographs of cross-sections of leather tanned with a mixture of DSA and DTAF–DSA. **(a)** H–DSA and DTAF–H–DSA were used. **(b)** M–DSA and DTAF–M–DSA were used. **(C)** L–DSA and DTAF–L–DSA were used

is in accordance with previous results regarding the penetration of enzymes[23,46] and acrylic resins.[26]

The results above demonstrated that the penetration behavior of fluorescent labeled dialdehyde polysaccharide tanning agent in leather matrix could be preliminarily visualized and semiquantified by using fluorescent tracing technique. In future research, high-resolution fluorescence microscopic techniques can be used to further observe the distribution of fluorescent labeled tanning agents within the hierarchical microstructure of leather. Thus, the issue of the multi-scale mass transfer and crosslinking of tanning agents in leather could be explored from a fresh perspective, and the tanning mechanism is expected to be deeply revealed.

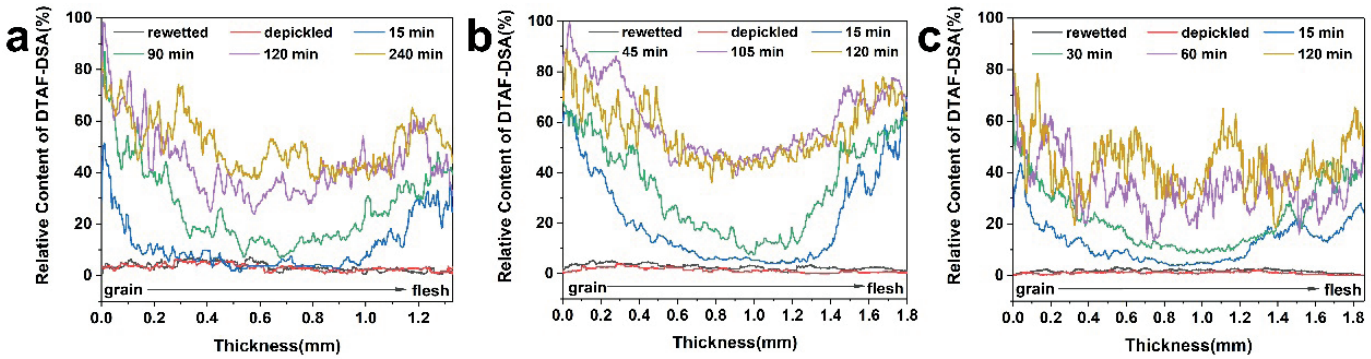

Figure 7. Distribution of **(a)** DTAF–H–DSA, **(b)** DTAF–M–DSA and **(c)** DTAF–L–DSA in the tanned leather. The relative contents of DTAF–DSA was quantified by analysis of the fluorescence micrographs in Figure 5 using Image J software

Conclusions

DSA tanning agent can be successfully labeled by fluorescein DTAF through covalent binding between hydroxyl of DSA and dichlorotriazine of DTAF. This provides a convenient fluorescent labeling method for polysaccharide-based tanning agents. Furthermore, the penetration and location of fluorescent labeled DSA tanning agent in leather can be visualized and preliminarily investigated by the fluorescent tracing technique. This provides an effective means to probe the mass transfer characteristics and help evaluate tanning effects of polysaccharide-based tanning agents. The results will help reveal the tanning mechanism and develop novel tanning agents.

Acknowledgement

This work was financially supported by the National Natural Science Foundation of China (22278280), Sichuan Science and Technology Program (2022JDRC0029), and the Tianfu Ten-thousand Talents Program of Sichuan Province.

References

1. Yu Y., Wang H., Wang Y. N., Zhou J. F., Shi B.; Construction of a Chrome-free Tanning System Based on Highly-oxidized Starch–Zirconium Complexes. *JALCA* **117**, 87-95, 2022.
2. Inbasekar C., Rao J. R., Fathima N.N.; Strategizing the Development of a Metal- and Formaldehyde-Free Tanning Process Using (3,5-Dimethyl-1H,3H,5H-oxazolo[3,4-c]oxazol-7a(7H)-yl) Methanol Heterocyclic Derivative Oxazolidine and Polyallylamine. *ACS Sustain. Chem. Eng.* **9**, 15053-15062, 2021.
3. Shen Y. M., Ma J. Z., Fan Q. Q., Gao D. G., Yao H.; Strategical development of chrome-free tanning agent by integrating layered double hydroxide with starch derivatives. *Carbohydr. Polym.* **304**, 120511, 2023.
4. Hedberg Y. S.; Chromium and leather: a review on the chemistry of relevance for allergic contact dermatitis to chromium. *J. Leather Sci. Eng.* **2**, 20, 2020.
5. Xu T., Jiang X. F., Tang Y. L., Zeng Y. H., Zhang W. H., Shi B.; Oxidation of trivalent chromium induced by unsaturated oils: a pathway for hexavalent chromium formation in soil. *J. Hazard. Mater.* **405**, 124699, 2021.
6. Xu T., Nan F., Jiang X. F., Tang T. L., Zeng Y. H., Zhang W. H., Shi B.; Effect of soil pH on the transport, fractionation, and oxidation of chromium (III). *Ecotox. Environ. Safe.* **195**, 110459, 2020.
7. Yu Y., Lin Y. R., Zeng Y. H., Wang Y. N., Zhang W. H., Zhou J. F., Shi B.; Life cycle assessment for chrome tanning, chrome-free metal tanning, and metal-free tanning systems. *ACS Sustain. Chem. Eng.* **9**, 6720-6731, 2021.
8. Guo X. R., Yu Y., Wang Y. N., Shi B.; Oxidized maltodextrin: a novel ligand for aluminum–zirconium complex tanning. *JALCA* **116**, 155-161, 2021.
9. Jiang Z. C., Ding W., Fan J. J., Liao Y. H., Remón J., Shi B.; Biomass derived oligosaccharides for potential leather tanning. *J. Leather Sci. Eng.* **5**, 7, 2023.
10. Chen H., Hu Y., Li S. Q., Chen L. W., Yi J., Shan Z. H., Dai R.; The tanning performance of dialdehyde cellulose prepared by electrochemical oxidation system. *J. Soc. Leather Thchnol. Chem.* **103**, 305-311, 2019.
11. Ding W., Yi Y. D., Wang Y. N., Zhou J. F., Shi B.; Peroxide-periodate co-modification of carboxymethylcellulose to prepare polysaccharide-based tanning agent with high solid content. *Carbohydr. Polym.* **224**, 115169, 2019.
12. Yi Y. D., Zhang Y., Mansel B., Wang Y. N., Prabakar S., Shi B.; Effect of dialdehyde carboxymethyl cellulose cross-linking on the porous structure of the collagen matrix. *Biomacromolecule* **23**, 1723-1732, 2022
13. Ozkan C. K., Ozgunay H., Akat H.; Possible use of corn starch as tanning agent in leather industry: Controlled (gradual) degradation by H2O2. *Int. J. Biol. Macromol.* **122**, 610-618, 2019..
14. Hao D. Y., Wang X. C., Liu X. H., Su R. R., Duan Z. J., Dang X. G.; Chrome-free tanning agent based on epoxy-modified dialdehyde starch towards sustainable leather making. *Green Chem.* **23**, 9693-9703, 2021.
15. Yu Y., Wang Y. N., Ding W., Zhou J. F., Shi B.; Preparation of highly-oxidized starch using hydrogen peroxide and its application as a novel ligand for zirconium tanning of leather. *Carbohydr. Polym.* **174**, 823-829, 2017.
16. Yu Y., Wang H., Wang Y. N., Zhou J. F., Shi B.; Chrome-free synergistic tanning system based on biomass-derived hydroxycarboxylic acid–zirconium complexes. *J. Clean Prod.* **336**, 130428, 2022.
17. Ding W., Zhou J. F., Zeng Y. H., Wang Y. N., Shi B.; Preparation of oxidized sodium alginate with different molecular weights and its application for crosslinking collagen fiber. *Carbohydr. Polym.* **157**, 1650-1656, 2017.
18. Ding W., Yi Y. D., Wang Y. N., Zhou J. F., Shi B.; Preparation of a highly effective organic tanning agent with wide molecular weight distribution from bio-renewable sodium alginate. *Chemistryselect* **3**, 12330-12335, 2018.
19. Ding W., Wang Y. N., Zhou J. F., Shi B.; Effect of structure features of polysaccharides on properties of dialdehyde polysaccharide tanning agent. *Carbohydr. Polym.* **201**, 549-556, 2018.
20. Nypelö T., Berke B., Spirk S., Sirvio J. A.; Review: Periodate oxidation of wood polysaccharides—Modulation of hierarchies. *Carbohydr. Polym.* **252**, 117105, 2021.
21. Yu Y., Zeng Y. H., Wang Y. N., Liang T., Zhou J. F., Shi B.; Inverse chrome tanning technology: a practical approach to minimizing Cr (III) discharge. *JALCA* **115**, 176-182, 2020.
22. Zeng Y. H., Yang Q., Wang Y. N., Zhou J. F., Shi B.; Neutral Protease Assisted Low-sulfide Hair-save Unhairing Based on pH-sensitivity of Enzyme. *JALCA* **111**, 345-353, 2016.
23. Song Y., Wu S. Q., Yang Q., Liu H., Zeng Y. H., Shi B.; Factors affecting mass transfer of protease in pelt during enzymatic bating process. *J. Leather Sci. Eng.* **1**, 4. 2019.

24. Wang H., Lei C., Zeng Y. H., Song Y., Zhang Q. X., Shi B.; Reversible inhibition of trypsin activity with soybean flour in hide bating process for leather quality improvement. *Ind. Crop. Prod.* **161,** 113222, 2021.
25. Zeng Y. H., Song Y., Li J., Zhang W. H., Shi B.; Visualization and Quantification of Penetration/Mass Transfer of Acrylic Resin Retanning Agent in Leather using Florescent Tracing Technique. *JALCA* **111**, 398-405, 2016.
26. Song Y., Zeng Y. H., Xiao K. L., Wu H. P., Shi B.; Effect of molecular weight of acrylic resin retanning agent on properties of leather. *JALCA* **112**, 128-134, 2017.
27. Song Y., Zeng Y. H., Shi B.; Effect of histological feature of leather on acrylic resin retanning. *J. Soc. Leather Technol. Chem.* **102**, 149-154, 2018.
28. Song Y., Wang Y. N., Zeng Y., Wu H. P., Shi B.; Quantitative determinations of isoelectric point of retanned leather and distribution of retanning agent. *JALCA* **113**, 232-238, 2018.
29. Huang W. L., Song Y., Yu Y., Wang Y. N., Shi B.; Interaction between retanning agents and wet white tanned by a novel bimetal complex tanning agent. *J. Leather Sci. Eng.* **2**, 8, 2020.
30. Du J. X., Shi L., Peng B. Y.; Real-time monitoring of the penetration of amphiphilic acrylate copolymer in leather using a fluorescent copolymer as tracer. *Microsc. Res. Tech.* **78**, 1146-1153, 2015.
31. Du J. X., Shi L., Peng B. Y.; Amphiphilic acrylate copolymer fatliquor for ecological leather: Influence of molecular weight on performances. *J. Appl. Polym. Sci.* **133**, 43440, 2016.
32. Wen H. M., Wang Y. L., Zhu H. X., Jin L. Q., Zhang F. F.; A Fluorescent Tracer Based on Castor Oil for Monitoring the Mass Transfer of Fatliquoring Agent in Leather. *Materials* **15**, 1167, 2022.
33. Song Y., Wu S. Q., Wang Y. N. Zhu M., Yi Y. D., Zeng Y. H., Shi B.; Visualization of penetration and reaction of aldehyde tanning agent in leather using fluorescence technique. *JALCA* **115**, 248-254, 2020.
34. Ding W., Wang Y. N., Zhou J. F., Liu H. T., Pang X. Y., Shi B.; Investigations on the general properties of biomass-based aldehyde tanned sheep fur for its selective post-tanning processing. *J. Leather Sci. Eng.* **3**, 5, 2021.
35. Liu, B. H., Wei, Z., Wang, Y. N., Shi, B.; Preparation of oxidized poly (2-hydroxyethyl acrylate) with multiple aldehyde groups by TEMPO-mediated oxidation for gelatin crosslinking. *JALCA,* **114,** 163-170, 2019.
36. Abitbol, T., Palermo, A., Moran-Mirabal, J. M.; Fluorescent labeling and characterization of cellulose nanocrystals with varying charge contents. *Biomacromolecules.* **14,** 3278–3284, 2013.
37. Li, Q. J., Yi, Y. D., Wang, Y. N., Li, J., Shi, B. Effect of cationic monomer structure on the aggregation behavior of amphoteric acrylic polymer around isoelectric point. *J. Leather Sci. Eng*, **4**, 4, 2022.
38. Fu, X., Dai, J. H., Guo, X. W., et al. Suppression of oligomer formation in glucose dehydration by CO_2 and tetrahydrofuran. *Green Chem.* **19,** 3334–3343, 2017.
39. Gupta, G. P., Nguyen, D. X., Chiang, A. C., Bos, P. D., Kim, J. Y., Nadal, C., Gomis, R. R., Manova-Todorova, K., Massague, J.; Mediators of vascular remodelling co-opted for sequential steps in lung metastasis. *Nature.* **446,** 765-770, 2007.
40. Wang, P., He, H. W., Cai, R., Tao, G., Yang, M. R., Zuo, H., Umar, A., Wang, Y. J.; Cross-linking of dialdehyde carboxymethyl cellulose with silk sericin to reinforce sericin film for potential biomedical application. *Carbohydr. Polym.* **212,** 403-411, 2019.
41. Khadiran, T., Hussein, M. Z., Zainal, Z., Rusli, R.; Shape-stabilised n-octadecane/activated carbon nanocomposite phase change material for thermal energy storage. *J. Taiwan Inst. Chem. Eng.* **55,** 189-197, 2015.
42. Wan, Y. C., Chen, Y., Cui, Z. X., Ding, H., Gao, S. F., Han, Z., Gao, J. K.; A promising form-stable phase change material prepared using cost effective pinecone biochar as the matrix of palmitic acid for thermal energy storage. *Sci Rep.* **9,** 11535, 2019.
43. De Hoog, P., Gamez. P., Driessen, W. L., Reedijk, J.; New polydentate and polynucleating N-donor ligands from amines and 2,4,6-trichloro-1,3,5-triazine. *Tetrahedron Lett.* **43,** 6783–6783, 2002.
44. Wang, Y. N., Huang, W. L., Zhang, H. S., Tian, L., Zhou, J. F., Shi, B.; Surface charge and isoelectric point of leather: A novel determination method and its application in leather making. *JALCA,* **112,** 224-231, 2017.
45. Wang, Y. N., Hu, L. Y.; Essential role of isoelectric point of skin/leather in leather processing. *J. Leather Sci. Eng*, **4,** 25, 2022.
46. Liu, C., Chen, X. Y., Zeng, Y. H., Shi, B.; Effect of the surface charge of the acid protease on leather bating performance. *Process Biochem.* **121,** 330-338, 2022.

Resource Utilization of Bovine Hair Recycling from Enzymatic Unhairing during Leather Manufacturing: Alkali-Protease Synergistic Preparation of Keratin and its in Vitro Antioxidant Activity

by

Ting Liu,[1,2] Chunxiao Zhang,[1,2]** Xu Zhang,[1,2] Biyu Peng[1,2]* and Mengchun Gao[1,2]

[1]*National Engineering Laboratory for Clean Technology of Leather Manufacture, Sichuan University*, Chengdu 610065, P. R. China;

[2]*Key Laboratory of Leather Chemistry and Engineering of Ministry of Education, Sichuan University*, Chengdu, Sichuan 610065, P. R. China)

Abstract

With the development of enzymatic unhairing technology in the leather industry, enhancing the recycling of bovine hair is a new issue emerging in leather-making. In this work, the effects of alkali concentration, time, and temperature in the pretreatment, as well as enzyme dosage, time, temperature, and pH in the following treatment on the dissolution performance and keratin yield of bovine hair were investigated. Hence, the extraction process of keratin from bovine hair by the alkali-enzyme method was optimized. The results show that the optimal conditions for the keratin extraction are as follows: for the pretreatment with alkali, the alkali concentration is 0.4 M, the pretreatment time is 1.0 h, the pretreatment temperature is 65°C, and for the following enzymatic treatment, the enzyme dosage is 3324 U/g bovine hair, the action time is 4.0 h, action temperature is 45°C, and the pH is controlled between 8.5-11.5. Compared with the alkali method, the alkali-enzyme method increases the keratin yield from 24.4% to 58.1%, and the alkali dosage is reduced by 50%. The prepared keratin had high in vitro antioxidant activity, which provided a new idea for the resource utilization of bovine hair waste.

Introduction

As the raw material of the leather industry is obtained from animal husbandry, leather making is the most feasible and sustainable way to solve the problem of recycling about 300 million pieces of bovine hide every year. In traditional leather processing, to achieve the purpose of unhairing and dispersing collagen fibers, a large amount of sulfide and lime is applied to remove hairs from hides and make hides swell.[1,2] This method has the advantages of convenient operation, easy control, and steady effect, and is widely used in the leather industry. However, due to the heavy use of sulfide and lime, the pollutant content generated by the dissolution of bovine hair in wastewater is high, and the emission loads of chemical oxygen demand (COD), sulfide, ammonia nitrogen, and total nitrogen in traditional unhairing are more than 30% of the whole leather processing.[3,4] With the advantages of being sustainable and eco-friendly, enzymatic unhairing technology is considered an effective way to reduce pollutant discharge in traditional unhairing. Moreover, after years of research and development, the safety and controllability of enzymatic unhairing technology have been effectively broken through, and it has gradually been widely applied in practical production.[5] Enzymatic unhairing technology can achieve a recovery of 80%–90% of bovine hair; and how to improve the high-value utilization efficiency of bovine hair is a new challenge for the leather industry.

Bovine hair is rich in keratin.[6] With good biocompatibility, skin friendliness, biodegradability, and physical and mechanical property, keratin has broad application prospects in protein composite film, regenerated fibers, food packaging material, leather functional material, cosmetic, and biomedical material.[7-9] In recent years, animal hair keratin extraction technology has developed rapidly. Wool, rabbit hair, pig hair, feather, and human hair have been applied for keratin extraction,[10, 11] but reports about keratin extraction using bovine hair as raw material are few. At present, the commonly used keratin extraction methods include mechanical grinding,[12] acid hydrolysis,[13] alkaline hydrolysis,[14] reduction,[15] oxidation,[16] enzymatic hydrolysis,[17] ionic liquid assisted method,[18] metal salt assisted method and copper–ammonia solution assisted method. The solubility of hair, the keratin yield, and the molecular weight, group, and chemical properties of keratin obtained from hair vary with different raw materials and extraction methods. In general, the keratin obtained by mechanical grinding under heating and pressurizing has a smaller molecular weight and is mainly used in the production of animal feed; the acid and alkaline hydrolysis method treat hair with a low solubility and obtain small molecular weight, while producing more neutral salts;[19] the keratin prepared by the reduction method has a large relative molecular weight with a narrow distribution and remains active sulfhydryl groups of cysteine to the maximum extent, but the shortcoming of this method is that the reducing agents used are mostly sodium sulfide, sodium bisulfite, sodium metabisulfite, and sulfhydryl compounds, all of which are toxic and easily cause secondary pollution to the environment.[20] The oxidation method has a relatively high solubility and a small relative

Manuscript received February 12, 2023, accepted for publication April 18, 2023.

*Corresponding Author e-mail: pengbiyu@scu.edu.cn; Tel.+86-28-85401208.

**Corresponding Author e-mail: chunxiaozhang@scu.edu.cn

molecular weight, and the common oxidants are mainly hydrogen peroxide, peroxyformic acid, peroxyacetic acid, and sodium hypochlorite, which also cause some environment problems, and the products generally need to be reduced with reducing agents;[16] the ionic liquid assisted method also has a high extraction rate and generally needs to be used with reducing agents.[18] The enzymatic hydrolysis method has the advantages of green, high efficiency, and mild reaction condition, which is one of the key research directions of keratin extraction technology from animal hair.

Nonspecific proteases and keratinases are used for the enzymatic hydrolysis method to obtain keratin from hair. Keratinase can break the disulfide bond. Thus, the extraction efficiency of keratin can be improved, but commercial keratinase is rare and the price is high.[21] Nonspecific proteases, commonly used for enzymatic extraction of hair keratin, enhance the efficiency of keratin extraction mainly by catalyzing the hydrolysis of peptide bonds in the keratin. However, nonspecific proteases do not break the disulfide bond of keratin, and the presence of the lipid-like layer outside the scale layer on the hair surface prevents the enzyme from contacting and penetrating the hair, which affects the catalytic action of the enzyme and decreases the extraction efficiency of keratin. Therefore, before enzymatic treatment, the hair is generally pretreated by oxidizing agents, reducing agents, alkalis, or other substances to destroy the lipid-like substances on the surface of the hair, improving the efficiency of enzymatic action.[22] The pretreatment protocols and enzymatic action conditions directly affect the solubility of hair, the extraction rate of keratin, and the relative molecular weights and structural characteristics of the extracted keratin samples.

In this work, the effects of alkali pretreatment conditions and enzymatic action conditions on the solubility and keratin yield of bovine hair were investigated to construct an efficient alkali–enzyme extraction. The research would provide a reference for improving the comprehensive utilization ratio of the bovine hair recovered by enzymatic unhairing in leather processing.

Materials and Methods

Materials

Alkaline protease (LKT, 280000 U/g, Shandong Lonct Enzymes Co., Ltd., China); bovine hair was obtained from Xuzhou Nanhai Tannery Co., Ltd., China, by the enzymatic unhairing process, and was washed with deionized water three times to remove dirt and blood, and dried at 105°C to constant weight; analytical grade chemicals were used in biochemical analysis.

Methods

Pretreating the bovine hair with differing concentration of NaOH before enzymatic hydrolysis

A 1.0 g sample of bovine hair was shake-incubated with 25.0 mL of NaOH solutions with concentrations of 0.2, 0.4, 0.8, 1.6, and 2.0 M at 65°C for 2.0 h, respectively. Then, the pH value of the mixture was adjusted to 11.5 with 6.0 M HCl solution. To this mixture, 3324 U of LKT protease per gram of bovine hair was added, and the reaction was kept at 55°C for 4.0 h by shaking incubator (water bath) (SHA-BA, Changzhou Aohua Instruments Co., Ltd., China). Subsequently, the enzyme was inactivated at 95°C for 10 min. The hydrolysate was rapidly cooled to room temperature and centrifuged at 10000 × g at 4°C for 20 min with high-speed refrigerated centrifuge (TGL-16M, Changsha Xiangyi Centrifuge Instruments Co., Ltd., China). The supernatant was dialyzed in deionized water for 48 h using a dialysis bag (350 Da, Millipore Co., Ltd. USA), and the deionized water was replaced every 12 h. After dialysis was completed, the dialysate was lyophilized to obtain the keratin (EKE) prepared by the alkali-enzyme method, using vacuum lyophilizer (FD-113-50, Beijing Boyikang Experimental Instruments Co., Ltd., China). The undissolved hair was repeatedly washed three times with deionized water and dried at 40°C to constant weight.

Effect of alkaline pretreating time on enzymatic hydrolysis of bovine hair

A 1.0 g portion of bovine hair was shake-incubated with 25.0 mL of NaOH solutions with concentrations of 0.4 M at 65°C for 0.5, 1.0, 2.0, 3.0 and 4.0 h, respectively. Then, the pH value of the mixture was adjusted to 11.5 with 6.0 M HCl solution. The other operations were performed as above.

Effect of alkaline pretreating temperature on enzymatic hydrolysis of bovine hair

A 1.0 g portion of bovine hair was shake-incubated with 25.0 mL of NaOH solutions with concentrations of 0.4 M at 35°C, 45°C, 55°C, 65°C and 75°C for 2.0 h, respectively. Other operations were the same as above.

Effect of protease dosage on enzymatic hydrolysis of bovine hair

A 1.0 g portion of bovine hair was shake-incubated with 25.0 mL of NaOH solutions with concentrations of 0.4 M at 65°C for 2.0 h. Then, the pH value of the mixture was adjusted to 11.5 with 6.0 M HCl solution. To this mixture, 416 U, 832 U, 1664 U, 3324 U, and 6648 U of LKT protease per gram of bovine hair was added, respectively, and the reaction was kept at 55°C for 4.0 h. Other operations were the same as above.

Effect of pH on enzymatic hydrolysis of bovine hair

After pretreatment with alkali, the pH value was adjusted to 8.5, 9.5, 10.5, 11.5, and 12.5, respectively, and the enzyme dosage was controlled to 3324 U/g for hydrolysis. The other operations were the same as above.

Effect of time on enzymatic hydrolysis of bovine hair

After the bovine hair was pretreated with alkali, the pH was adjusted to 11.5 and treated with 3324 U/g of protease at 55°C for 2.0, 3.0, 4.0, 5.0, and 6.0 h, respectively. Other operations were the same as above.

Table I

Horizontal table of orthogonal experimental factors

Level	Alkali concentration (M)	Alkali pretreatment time (h)	Enzyme dosage (U/g)	Enzymatic treatment time (h)
	A	B	C	D
1	0.2	1.0	1662	2.0
2	0.4	2.0	3324	3.0
3	0.8	3.0	6648	4.0

Effect of temperature on enzymatic hydrolysis of bovine hair

After the bovine hair was pretreated with alkali, the pH was adjusted to 11.5 and treated with 3324 U/g of protease at 35°C, 45°C, 55°C, 65°C, and 75°C, and the other operations were the same as above.

Orthogonal experiments for hydrolysis of bovine hair by alkali-enzyme synergy

According to the optimization results of the single-factor test, a four-factor and three-level orthogonal experiment was conducted to further optimize the alkali-enzyme method conditions. The extraction ratio of keratin was considered as the response value, and the alkali concentration, enzyme dosage, enzymatic treatment time, and enzyme treatment temperature were considered as the response factors.

Determination of bovine hair solubility and keratin extraction rate

$$\text{Bovine hair solubility (\%)} = \frac{W_1}{W_0} \times 100\%$$

$$\text{Keratin extraction rate (\%)} = \frac{W_0 - W_2}{W_0} \times 100\%$$

W_0: weight of initial bovine hair, g; W_1: weight of bovine hair keratin after freeze-drying, g; W_2: weight of insoluble material after hydrolysis of bovine hair, g.

Determination of molecular weight

The molecular weight distribution of bovine hair hydrolysate was measured by gel filtration chromatography (GPC) and Sodium dodecyl sulfate-polyacrylamide gel electrophoresis (SDS-PAGE).

GPC analyzation: 100.00 mg freeze-dried bovine hair hydrolysate was dissolved in 10.00 mL deionized water in volumetric flask, filtered through a 0.22 um filter. Then, the molecular weights of the hydrolysates were analyzed by Agilent 1260 Infinity II HPLC system and TSK gel G2000 SWXL column (7.8 mm × 300 mm) as the conditions reported before,[23] by using the mobile phase: 0.05 M, pH=7.0 NaH_2PO_4-Na_2HPO_4+0.15 M NaCl buffer.

SDS-PAGE analyzation: The hydrolysates solution was prepared at 10 mg/m L, and SDS-PAGE was performed using 12% separating gel, and after the end of the process, it was stained with Kormas Brilliant Blue R250 and decolorized with acetic acid-ethanol solution.

Analysis of amino acid composition of bovine hair keratin

A 50 mg portion of freeze-dried keratin powder was taken in a digestion tube, and 4 mL of 6 M HCl was added in it. After digesting at 120°C for 24 h, the sample solution was concentrated and evaporated to dryness.[24] After diluting to 100.00 mL with deionized water, the solution was filtered through the 0.22 μm filter membrane. The concentration of each amino acid in the hydrolyzate was determined with an amino acid analyzer.

Determination of DPPH scavenging activity

A 2.0 mL aliquot of ethanol solution containing 25.0 μg/mL DPPH was well-mixed with 2.0 mL of keratin solutions with different concentrations, respectively. The reaction was carried out in the dark at room temperature for 60 min, then measuring the absorbance of the mixture at 517 nm.[25] Meanwhile, 2.0 mL of ethanol solution and 2.0 mL of keratin solutions were mixed as blank, and 2.0 mL of ethanol solution containing DPPH and 2.0 mL of deionized water were mixed as control. The DPPH free radical scavenging activity was calculated according to the following equation.

$$DPPH\ (\%) = 1 - \frac{A_s - A_c}{A_b} \times 100\%$$

A_s is the absorbance of the keratin solution mixed with DPPH solution; A_c is the absorbance of the keratin solution mixed with ethanol; A_b is the absorbance of the DPPH solution mixed with deionized water.

Determination of ABTS scavenging activity

A 0.4 ml volume of keratin solutions with different concentrations were mixed with 3.6 mL of fresh 2,2'-Azinobis-(3-ethylbenzthiazoline-6-sulphonate) diammonium salt (ABTS) solution with an absorbance value of 0.7±0.02 (OD_{734}), and the mixture was kept in the dark at room temperature for 5 min, measuring the absorbance of the mixture at 734 nm.[26] Deionized water and reduced glutathione were alternatives of samples as the negative and positive control, respectively. The ABTS free radical scavenging activity was calculated according to the following equation.

$$ABTS\ (\%) = 1 - \frac{A_b - A_S}{A_b} \times 100\%$$

A_b is the absorbance of deionized water mixed with ABTS solution; A_s is the absorbance of the keratin solution mixed with ABTS solution.

Unless otherwise indicated, three replicate assays were conducted in all experiments, and the results were expressed as the average ± standard.

Results and Discussion

The alkali–enzyme extraction of keratin from bovine hair consisted of two steps: pretreatment with alkali and enzymatic treatment. The extraction was optimized by investigating the effect of process conditions on the solubility and the yield of keratin.

Optimization of alkali pretreatment parameters

Effect of alkali concentration

The NaOH concentrations were 0.2, 0.4, 0.8, 1.6, and 2.0 M. After pretreatment at 65°C for 2.0 h, the pH of the reaction mixture was adjusted to 11.5, and 3324 U of LKT protease per gram of bovine hair was added. Then, the reaction was kept at 55°C for 4.0 h. The results are shown in Figure 1.

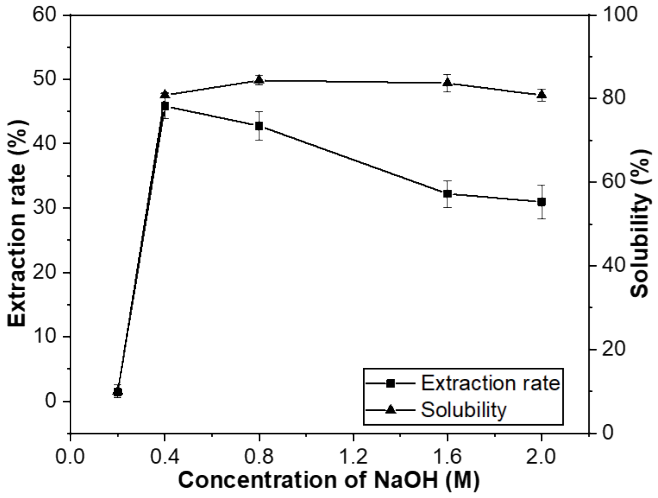

Figure 1. Effect of NaOH concentration on the solubility and keratin yield

Figure 1 shows the solubility and the keratin yield increases gradually as the NaOH concentration increases. When the NaOH concentration increases to 0.4 M, the solubility stabilizes, but the keratin yield decreases. This is mainly due to the scale layer of bovine hair contains many lipid-like materials and disulfide bonds with the hard structure, which makes the hair hydrophobic and resistant to enzymatic hydrolysis.[27] The pretreatment with NaOH can destroy the scale layer of the bovine hair surface and make it more hydrophilic, which is beneficial to improving the efficiency of the enzymatic action. However, as shown in Figure 2 and Table II, both the molecular weight of the bovine hair hydrolysates and their distributions (PD) would decrease when the concentration of sodium hydroxide reached more than 0.4 M in alkaline treatment. This could be attributed to that, when the concentration of alkali is too high, the hydrolysis of the peptide bonds in proteins would be accelerated and the higher molecular keratin would be further hydrolyzed into the low molecular components, producing the smaller molecule peptides, amino acids. Moreover, the dialysis treatment removed most of the small molecular hydrolysates, including amino acids, increasing the loss rate of keratin and decreasing the keratin yield. Therefore, the NaOH concentration should be about 0.4 M during pretreatment.

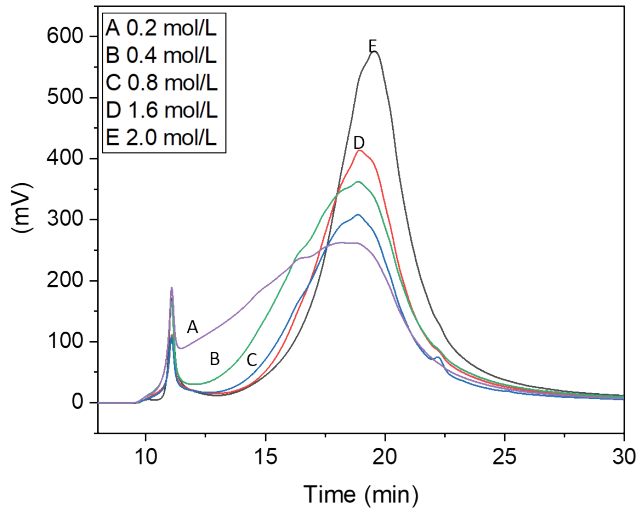

Figure 2. GPC gel chromatogram of keratin with differing NaOH concentration

Table II

Molecular weight distribution of keratin with differing NaOH concentration*

Concentration (M)		Percentage (%)	Mn/Da	Mw/Da	PD
0.2	1	5	67927	68017	1.00
	2	95	7392	35872	4.85
0.4	1	1	68620	68620	1.00
	2	99	7293	27189	2.66
0.8	1	3	66910	67025	1.00
	2	97	12304	23195	1.17
1.6	1	3	66731	66907	1.00
	2	97	7757	20693	1.99
2.0	1	3	66046	66143	1.00
	2	97	8308	18075	1.88

*: Mn is the number-average molecular weight, Mw is the weight-average molecular weight, PD is the molecular weight distribution coefficient, representing Mw/Mn

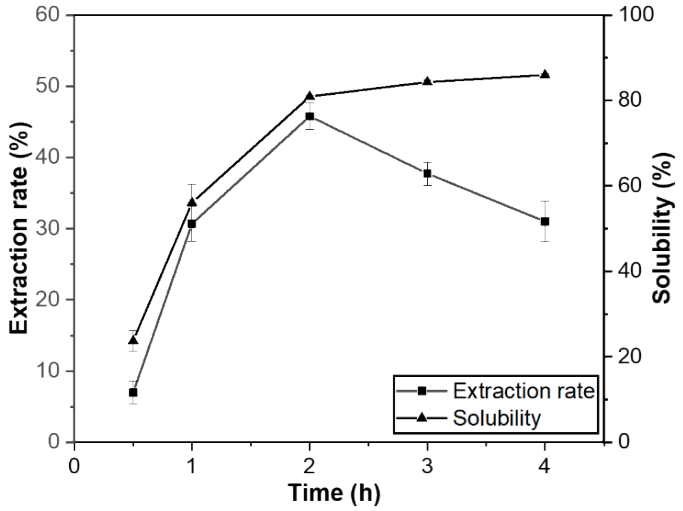

Figure 3. Effect of pretreatment time with NaOH on the solubility and keratin yield

Effect of pretreatment time with alkali

To investigate the effect of pretreatment time with alkali, the NaOH concentration was 0.4 M, and reactions were conducted at 65°C for 0.5, 1.0, 2.0, 3.0, and 4.0 h. The results are shown in Figure 3.

Figure 3 shows when the pretreatment time with alkali reaches 2.0 h, the solubility of bovine hair gradually stabilizes, and the yield of keratin gradually decreases. When the pretreatment time exceeds 2.0 h with 0.4 M NaOH solution, the peptide bond of keratin begins to be hydrolyzed by alkali, and the yield of keratin is affected by the formation of hydrolysis products with low molecular weights.

Effect of pretreatment temperature with alkali

To investigate the effect of pretreatment temperature with alkali, the NaOH concentration was 0.4 M, and reactions were conducted at 45°C, 55°C, 65°C, 75°C, and 85°C for 2.0 h. The results are shown in Figure 4.

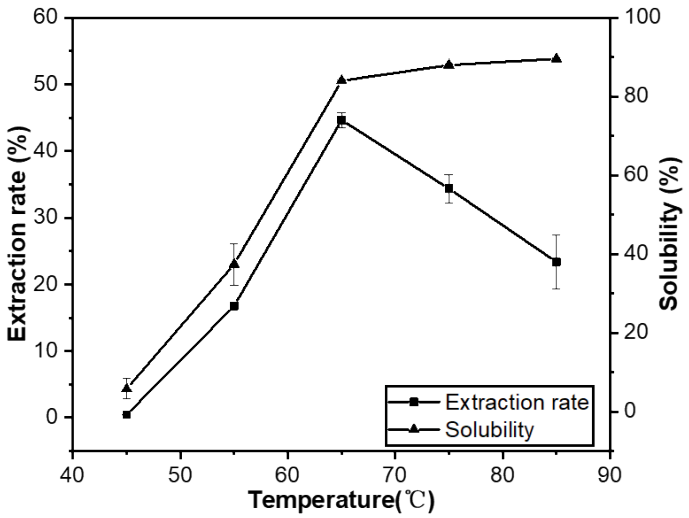

Figure 4. Effect of pretreatment temperature with NaOH on the solubility and keratin yield

Figure 4 shows that with the increase in pretreatment temperature, the solubility of bovine hair shows a trend of increasing and then stabilizing, but the keratin yield shows a trend of increasing and then decreasing. When the temperature is higher than 65°C, the keratin yield decreases sharply. On the one hand, the increase in pretreatment temperature helps make the keratin fiber swell fully. On the other hand, it causes the intense hydrolysis of the keratin peptide bond, resulting in a sharp decrease in keratin yield. Moreover, the excessive temperature makes controlling the temperature in the later enzymatic treatment more difficult. Therefore, the pretreatment temperature with alkali should be 65°C.

Optimization of enzymatic hydrolysis parameters

Effect of enzyme dosage

After pretreatment with 0.4 M NaOH solution at 65°C for 2.0 h, the pH of the reaction mixture was adjusted to 11.5 with 6.0 M HCl solution. Then, to investigate the effect of enzyme dosage, protease was added at different concentrations of 416, 832, 1664, 3324, and 6648 U per gram of bovine hair, and reactions were conducted at 55°C for 4.0 h. The results are shown in Figure 5.

Figure 5 shows the increase of enzyme dosage from 416 U/g to 6648 U/g has no substantial effect on the solubility of bovine hair, but the keratin yield shows a trend of increasing and then decreasing because the protease can effectively enter the interior of the bovine hair fiber and hydrolyze the peptide bond after pretreatment with alkali. When the enzyme concentration increases to about 3324 U/g, it can make the reaction of the enzyme and keratin reach better conditions. When the enzyme dosage further increases, it causes the excessive hydrolysis of the peptide bond and affects the final yield of keratin. As the dosage of enzyme increases, the enzyme protein content in the keratin also increases, which affects the purity of keratin. Therefore, the enzyme concentration should be 3324 U/g.

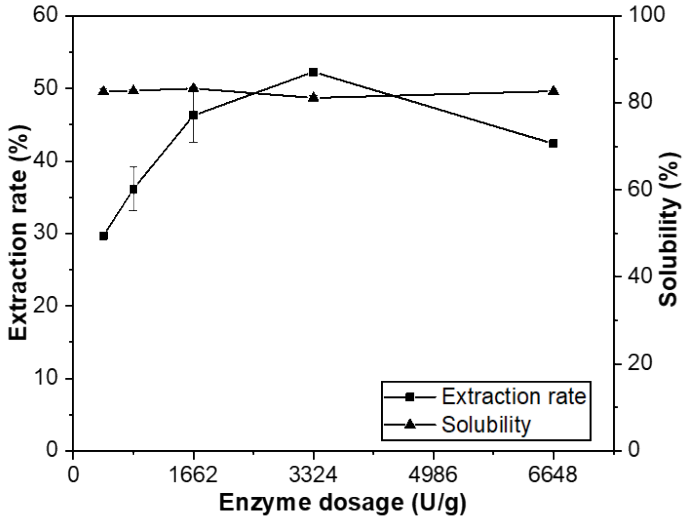

Figure 5. Effect of enzyme dosage on the solubility and keratin yield

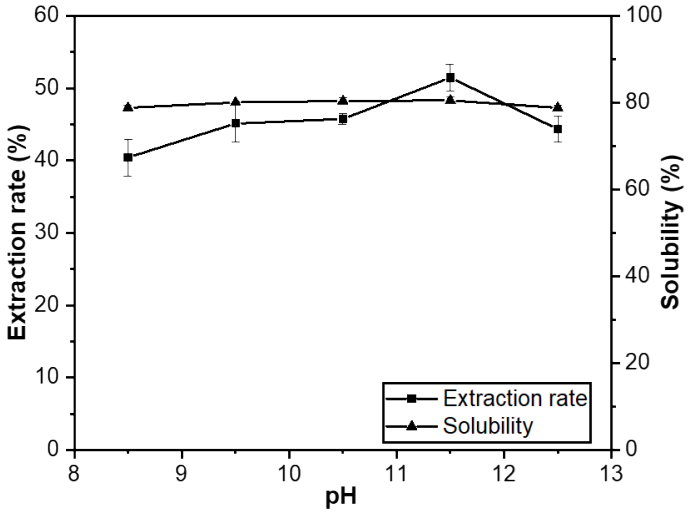

Figure 6. Effect of pH of enzymatic treatment on the solubility and keratin yield

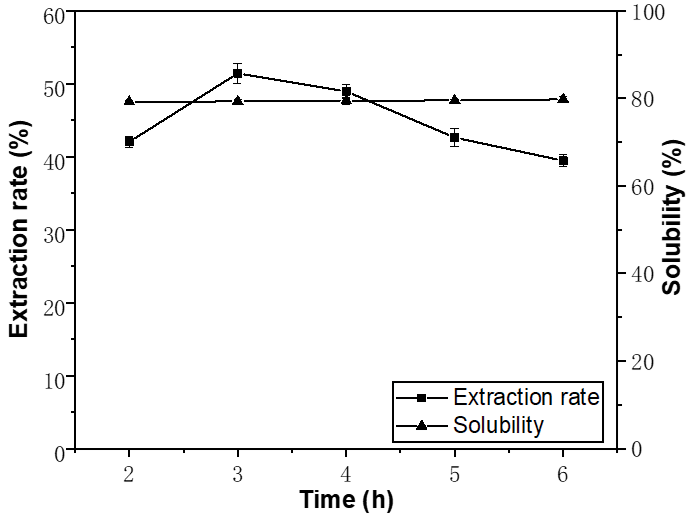

Figure 7. Effect of time of enzymatic treatment on the solubility and keratin yield

Effect of pH of enzymatic treatment

After the pretreatment with alkali, the pH values of reaction mixtures were adjusted to 8.5, 9.5, 10.5, 11.5, and 12.5 with 6.0 M HCl solution, and then treated with 3324 U/g (based on the enzyme activity at pH 11.5, and the same below) of protease at 55°C for 4.0 h. The results show that when the enzyme dosage is 3324 U/g, the change in pH does not have a considerable effect on the solubility of bovine hair and keratin yield, which are stable at about 80% and 45%, respectively, because the stability of the enzyme activity is better in the range of pH 8.5–12.5, and the enzyme dosage is high. Therefore, the pH has no remarkable effect on keratin hydrolysis.

Effect of time of enzymatic treatment

After pretreatment with alkali, the pH values of reaction mixtures were adjusted to 11.5, and each mixture was added 3324 U/g of the enzyme. Subsequently, reactions were conducted at 55°C for 2.0, 3.0, 4.0, 5.0, and 6.0 h. The results are shown in Figure 7. Under the above conditions, the increase of enzymatic treatment time has no substantial effect in the solubility of bovine hair, but the extraction rate of keratin increases slightly and then decreases gradually because the enzymatic hydrolysis of bovine hair is carried out in steps. In the initial stage of enzymatic treatment, the enzyme is affected by the adsorption of keratin fibers and mainly hydrolyzes the peptide bonds of undissolved fibrillar keratin, thus enhancing the solubility of bovine hair. When the hair is completely dissolved, the enzyme continues to act on the soluble keratin and further hydrolyzes keratin peptide bonds, which further reduces the molecular weight of soluble keratin and even generates peptides with low molecular weights and amino acids. Therefore, when the enzymatic treatment time exceeds about 3.0 h, the yield of keratin starts to decrease remarkably. Therefore, to ensure a high yield of keratin, the enzymatic treatment time should be about 3.0 h.

Effect of temperature of enzymatic treatment

After pretreatment with alkali, the pH of the reaction mixture was adjusted to 11.5, and 3324 U/g of the enzyme was added. To investigate the effect of temperature on the enzymatic treatment further, reactions were conducted at 35°C, 45°C, 55°C, 65°C and 75°C for 3.0 h. The results are shown in Figure 8.

Figure 8 shows that the temperatures below 45°C have no substantial effect on the solubility and the keratin extraction rate. Temperatures higher than 45°C also have no considerable effect on the dissolution rate, but the keratin yield gradually decreases. When the temperature is higher (under higher pH conditions), although the enzyme activity is inhibited or even inactivated, the protein becomes alkaline hydrolyzed. Therefore, the keratin further hydrolyzes to form peptides with low molecular weights and amino acids, affecting the keratin yield. The maximum keratin yield is obtained when the enzymatic treatment temperature is about 45°C.

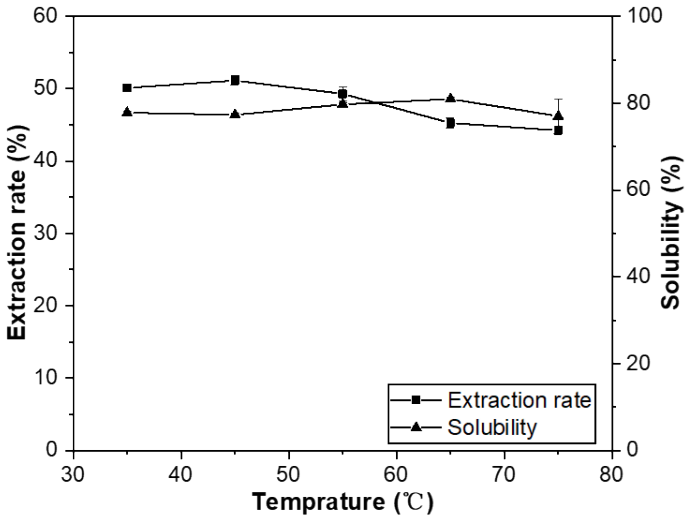

Figure 8. Effect of temperature of enzymatic treatment on the solubility and keratin yield

Optimization of orthogonal experiment

According to the result of the single-factor experiment, the optimal conditions for the keratin extraction of bovine hair by the alkali-enzyme method are as follows: For the pretreatment with alkali, the NaOH concentration is 0.4 M, and the pretreatment time and temperature cannot exceed 2.0 h and 65°C, respectively. For the following enzymatic treatment, the enzyme dosage, pH, and time are 3324 U/g, 8.5–12.5, and around 3.0 h, respectively, and the treatment temperature cannot exceed 45°C. Four factor variables were further selected as follows: alkali concentration (A), alkali treatment time (B), enzyme dosage (C), and enzyme treatment time (D). A four-factor and three-level orthogonal experiment was conducted to investigate the optimal conditions for keratin preparation. The results in Table III show the main order of the four key factors affecting the keratin extraction rate is alkali concentration of pretreatment > alkali pretreatment time > enzyme dosage > enzyme treatment time. The optimal conditions of the experiment can be obtained as follows: A2B1C2D3, that is, the NaOH concentration, pretreatment time, enzyme dosage, and enzymatic treatment time are 0.4 M, 1.0 h, 3324 U/g, and 4.0 h, respectively. Thus, the keratin extraction rate is 61.21%, which is similar to the results obtained from the single-factor optimization experiment. The best combination of enzymatic hydrolysis by calculating the K value is A2B1C3D3, that is, the NaOH concentration, pretreatment time, enzyme dosage, and enzymatic treatment time are 0.4 M, 1.0 h, 6648 U/g, and 4.0 h, respectively. The keratin extraction rate is 62.46%, which is greater than the results of the nine experiments in the orthogonal experiment. Owing to the double amounts of enzyme, the extraction rate only increases by 1.0%. Therefore, A2B1C2D3 is selected as the optimal reaction condition.

Table IV shows that compared with the conventional alkaline hydrolysis method reported in the literature[28] and the optimized alkaline pretreatment conditions lacking only the enzyme, the alkali–enzyme synergistic hydrolysis method can reduce the amount of alkali from 80.0% to 40.0%, and the acid dosage used for adjusting pH also decreases from 73% to 43.0%. Although the bovine hair solubility of the alkali–enzyme method is lower than that of the alkaline hydrolysis method, the extracted keratin yield increases from 24.4% to 58.1% because the dissolved keratin is easily hydrolyzed into amino acids and other products with low molecular weight when the alkali concentration is high, resulting in the loss of keratin.

Table III

Results of orthogonal experiment of keratin preparation obtained from bovine hair by alkali-enzyme method

Number	A	B	C	D	Extraction rate /%
1	1	1	1	1	1.21
2	1	2	2	2	1.59
3	1	3	3	3	2.92
4	2	1	2	3	61.21
5	2	2	3	1	58.35
6	2	3	1	2	55.36
7	3	1	3	2	55.29
8	3	2	1	3	51.26
9	3	3	2	1	48.26
K1	5.72	127.71	117.83	117.82	
K2	174.92	121.20	121.06	122.24	
K3	154.81	116.54	126.56	125.39	
k1	1.91	42.57	39.28	39.27	
k2	58.31	40.40	40.35	40.75	
k3	51.60	38.85	42.19	41.80	
Range	52.90	3.72	2.91	2.52	
Order-Sequence	A>B>C>D				
Optimal Level	A2	B1	C3	D3	
Optimal Combination	A2B1C3D3				

Table IV

Comparison of keratin extraction of alkali-enzyme and alkaline hydrolysis method

Method	Alkali dosage /%	Acid dosage /%	Solubility/%	Keratin yield/%
Alkaline hydrolysis*	80.0	73.0	90.0	24.4
Alkali-Enzyme hydrolysis**	40.0	43.0	72.1	58.1
Alkaline pretreatment***	40.0	43.0	33.9	16.8

*Alkaline hydrolysis conditions (AKE): 0.8 M NaOH, 1:25 solid-liquid ratio of, 65°C, 4.0 h.[28]

**Alkali-enzyme hydrolysis conditions (EKE): for pretreatment, 0.4 M NaOH, 1:25 solid-liquid ratio, 65°C, and 1.0 h are selected; for enzymatic treatment, when the reaction mixture is cooling down to 45°C, the pH of the mixture is adjusted to 11.5, and the reaction is conducted for 4.0 h by adding 3324 U/g of the protease.

***Alkaline pretreatment: 0.4 M NaOH, 1:25 solid-liquid ratio, 65°C, and 1.0 h are selected; then, when the reaction mixture is cooling down to 45°C, the pH of the mixture is adjusted to 11.5, and the reaction is conducted for 4.0 h.

Analysis and evaluation of the keratin extracted from bovine hair

Molecular weight and distribution of keratin

Studies have shown that the molecular weight of bovine hair hydrolyzed keratin affects its application properties, therefore the molecular weight and distribution of bovine hair hydrolyzed products were analyzed by gel filtration chromatography (GPC) after dialysis, concentration and drying, and the results are shown in Figure 9 and Table V.

Bovine hair keratin has many intermolecular crosslinks and is a large molecular protein. Upon alkali or alkali-enzyme hydrolysis, keratin undergoes cleavage of peptide bonds. Both bovine hair hydrolysis products (after dialysis) have two main fractions, consisting of proteins with molecular weights (Mw) in the range of 35.6 kDa-66.7 kDa Da. The content of fractions around 65.9 kDa was 18.55% in AKE and 81.45% in Mw of 43.5 kDa; the content of fractions around 66.7 kDa was 2.95% in AKE and 97.05% in Mw of 35.6 kDa. The proportion of higher molecular weight fractions in both bovine hair keratin was low. In alkali-hydrolyzed keratin, the content of the large molecular weight fraction was significantly higher than that of the enzymatic digestion product, probably because of specific cleavage and efficient catalysis by the enzyme. The low molecular weight fraction of EKE accounted for the majority of the fraction and had a lower molecular weight than the AKE. The results of SDS-PAGE analyzation in Figure 9 further show that the final keratin produced from bovine hair by both alkaline and alkaline-enzyme method contains protein components with continuous molecular weight distribution. This is consistent with the

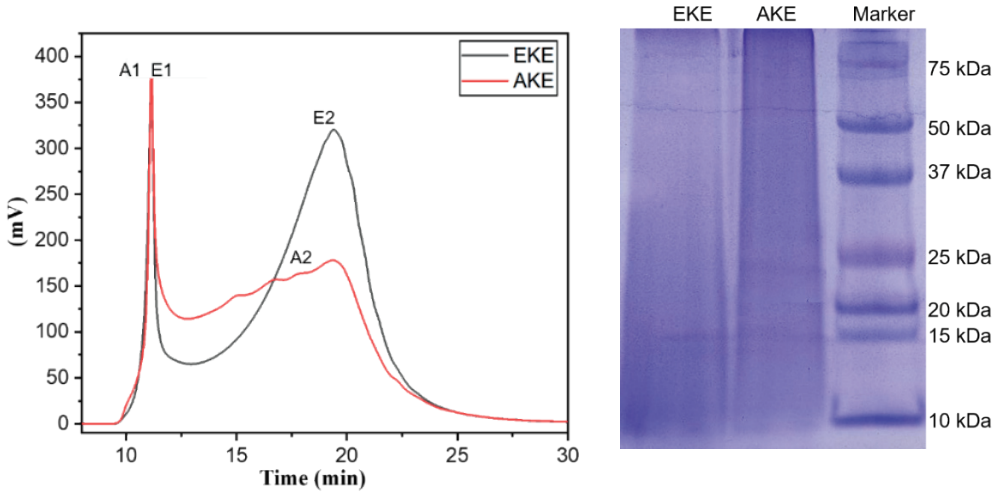

Figure 9. GPC gel chromatogram and SDS-PAGE of keratin

Table V

Molecular weight distribution of keratin

Sample		Percentage (%)	Mn/Da	Mw/Da	PD
AKE	1	18.55	65817	65913	1.00
	2	81.45	37642	43548	1.16
EKE	1	2.95	66643	66714	1.00
	2	97.05	25181	35639	1.41

Table VI

Analysis of amino acid composition of bovine hair and keratin (mg/100 mg)

Amino acid type	HAA*	BAA**	AAA***	TAA****
Bovine hair	35.67	12.97	5.18	53.82
EKE	32.55	11.94	4.20	48.69
AKE	31.52	15.36	3.93	50.81
Cottonseed Protein Peptide[30]	22.58	12.19	5.99	40.76
Okra Protein Peptide[31]	32.00	9.22	1.02	42.24

*HAA-total hydrophobic amino acids (Gly, Ala, Val, Pro, Phe, Leu, Ile, Met);

**BAA-total alkaline amino acids (Arg, Lys, His);

***AAA-total aromatic amino acids (Phe, Tyr);

****TAA-total amino acids affecting antioxidant properties.

results of GPC, for the PD was larger than 1.0. This could be attributed to the fact that the hydrolysis sites of the protein peptide bonds by alkaline are random, and the LKT protease can catalytic hydrolysis for the peptide bonds formed by most amino acids.

Amino acid composition of bovine hair keratin

Antioxidants are an important area of application for protein hydrolysis products. Studies have shown that hydrophobic, alkaline and aromatic amino acids can act as good electron donors to scavenge free radicals and enhance the antioxidant properties of protein products.[29] Therefore, the content of amino acids related to antioxidant properties in the prepared bovine hair keratin was analyzed and compared with protein peptides with good antioxidant properties reported. Table VI shows that the amino acid content of bovine hair hydrolysates related to antioxidant properties ranged from 48.96 mg/100 mg to 50.81 mg/100 mg, which was significantly higher than the cottonseed protein peptide and okra Protein peptides.[30,31] It can be speculated that bovine hair keratin products have higher antioxidant properties.

DPPH free radical scavenging ability

1,1-diphenyl-2-trinitrophenylhydrazine (DPPH) is a stable free radical and is widely used to assess the free radical scavenging ability of protein hydrolysates, peptides, and other substances.[32]

As seen in Figure 10 and Table VII, both AKE and EKE show a good free radical scavenging ability and the scavenging rate increases with the increase in peptide concentration. EKE and AKE have the IC_{50} value of 1.16 mg/mL and 1.51 mg/mL, respectively, and the IC_{50} of positive control GSH was 0.39 mg/mL. Although the DPPH free radical scavenging capacity of keratins were lower than the GSH, it is significantly higher than elastin peptides, whose IC_{50} value is 4.86 mg/mL.[33] In addition, the scavenging capacity of EKE for DPPH radicals was higher than AKE, mainly because AKE contains more randomly curled structures, which affects its antioxidant properties.[31]

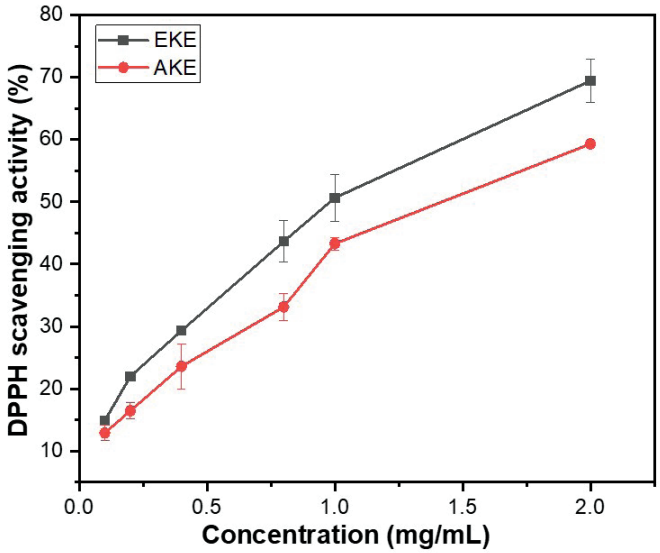

Figure 10. DPPH free radical Scavenging abilities of keratin under different concentrations

Table VII

DPPH free radical Scavenging abilities of keratin under different concentrations

Sample	Regression equation	R^2	IC_{50}(mg/mL)
AKE	y = 0.2462x + 0.1298	0.9676	1.51
EKE	y = 0.2813x + 0.1723	0.9572	1.16

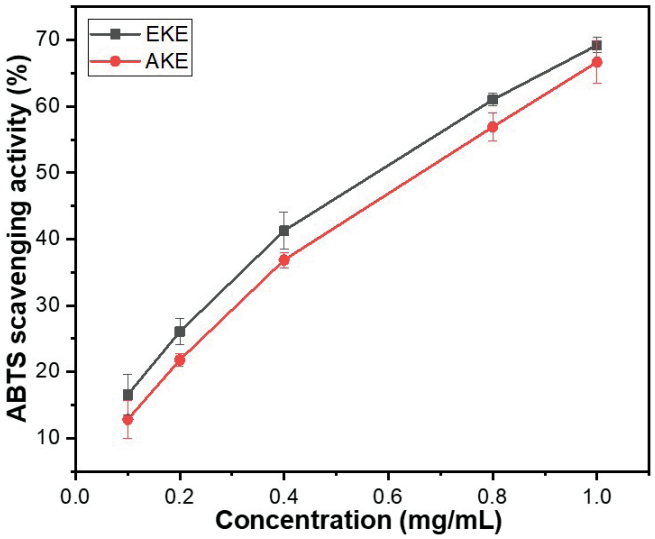

Figure 11. ABTS free radical Scavenging abilities of keratin under different concentrations

Table VIII

ABTS free radical Scavenging abilities of keratin under different concentrations

Sample	Regression equation	R^2	IC_{50}(mg/mL)
AKE	y = 0.5471x + 0.0951	0.9869	0.74
EKE	y = 0.5724x + 0.1421	0.9826	0.63

ABTS free radical scavenging ability

2,2-biazo-bis (3-ethyl-benzothiazole-6-sulfonic acid) diammonium salt (ABTS) is a positively charged free radical that can acquire an electron from the antioxidant molecule to form a stable neutral molecule and has been widely used for the antioxidant activity assay.

As seen in Figure 11 and Table VIII, both bovine hair keratin AKE and EKE have significant scavenging effects on ABTS radicals, and their scavenging ability increase in a dose-dependent way when the concentration of keratin increases to 1.0 mg/mL, the ABTS free radical scavenging rate of EKE and AKE is 65%-70%. The IC_{50} values of the scavenging capacity of keratin for ABTS obtained from the two hydrolysis methods were 0.74 mg/mL and 0.63 mg/mL, both higher than the glutathione (0.54 mg/mL). The scavenging capacity of keratin for ABTS was weaker than the glutathione, but both were stronger than that of the bovine hair hydrolysate reported.[34]

Conclusion

Enzymatic unhairing technology have been gradually widely applied in practical production, and the tanneries are concerned about how to improve the solubility and keratin yield of the recycled bovine hair, and the basic application properties such as the antioxidant properties of the resulting keratin. The work in this paper reports the synergistic effect of enzyme and alkali in keratin extraction from hair wastes generated by leather industry. The optimal conditions for the bovine hair keratin preparation by the alkali-enzyme method were obtained by single-factor and orthogonal experiments: the NaOH concentration, pretreatment time, pretreatment temperature, enzyme dosage, enzymatic treatment time, enzymatic treatment temperature, and enzymatic treatment pH are 0.4 M, 1.0 h, 65°C, 3324 U/g, 4.0 h, 45°C, and pH 11.5, respectively. Under these conditions, the keratin extraction rate was 61.21%. Compared with the alkali treatment, the alkali-enzyme treatment reduced the alkali dosage and improved the dissolution rate, which complied with the solid waste principle. Moreover, the prepared keratin had high in vitro antioxidant activity. The synergistic method successfully increases the bovine hair, the keratin yields and the antioxidant activity of keratin, which provided a new idea for the resource utilization of bovine hair waste.

Acknowledgements

This work was financially supported by National Natural Science Foundation of China (21908149), China Postdoctoral Science Foundation (2018T110974, 2018M633366), National Key R&D Program of China (2017YFB0308402), and the Fundamental Research Funds for the Central Universities (2023SCU12104).

References

1. Aquim P M D, Gutterres M., Trierweiler J. Assessment of water management in tanneries: State of RioGrande do Sul case study. *Journal of Society of Leather Technologists and Chemists* **94**, 253-258, 2010.
2. Jian S., Tao W., Chen W. Kinetics of enzymatic unhairing by protease in leather industry. *Journal of Cleaner Production* **19**, 325-331, 2011.
3. Dixit S., Yadav A., Dwivedi P. D., et al. Toxic hazards of leather industry and technologies to combat threat: a review. *Journal of Cleaner Production* **87**, 39-49, 2015.
4. Dettmera A., Cavallia É., Ayubb M. A., et al. Environmentally friendly hide unhairing: enzymatic hide processing for the replacement of sodium sulfide and delimig - ScienceDirect. *Journal of Cleaner Production* **47**, 11-18, 2013.
5. Chen M., Jiang M. F., Chen M., et al. Approach towards safe and efficient enzymatic unhairing of bovine hides. *JALCA* **113**, 59-64, 2018.
6. Segoviano-Garfias José J. N., Elena L., Padilla-Rizo B., et al. Recycling of animal by-products: composition and nutritional value of hydrothermally hydrolyzed bovine hair. *Revista de Ciencias Ambientales* **54**, 92-110, 2020.
7. Feroz S., Muhammad N., Ranayake J., et al. Keratin - Based materials for biomedical applications. *Bioactive Materials* **5**, 496-509, 2020.
8. Ramirez D. S., Carletto R. A., Tonetti C., et al. Wool keratin film plasticized by citric acid for food packaging. *Food Packaging and Shelf Life* **12**, 100-106, 2017.
9. Zoccola M., Aluigi A., Tonin C. Characterisation of keratin biomass from butchery and wool industry wastes. *Journal of Molecular Structure* **938**, 35-40, 2009.
10. Wang D., Yang X. H., Tang R. C., et al. Extraction of keratin from rabbit hair by a deep eutectic solvent and its characterization. *Polymers* **10**, 993, 2018.
11. Bayramoglu E. E., Yorgancioglu A., Yeldiyar G., et al. Extraction of keratin from unhairing wastes of goatskin and creating new emulsion formulation containing keratin and calendula flower (calendula officinalis L.). *JALCA* **109**, 49-55, 2014.
12. Papadopoulos M. C., Boushy A. E., Roodbeen A. E., et al. Effects of processing time and moisture content on amino acid composition and nitrogen characteristics of feather meal. *Animal Feed Science & Technology* **14**, 279-290, 1986.
13. Jing Z., Yi L., Li J., et al. Isolation and characterization of biofunctional keratin particles extracted from wool wastes. *Powder Technology* **246**, 356-362, 2013.
14. Shaobo X. U., Liu Q., Zhang J., et al. Study on the extraction of human hair keratin and subcutaneous implantation experiment of animal. *Clinical Medicine & Engineering* **21**, 1527-1528, 2014.
15. Alahyaribeik S., Ullah A.. Methods of keratin extraction from poultry feathers and their effects on antioxidant activity of extracted keratin. *International Journal of Biological Macromolecules* **148**, 449-456, 2020.
16. Shavandi A., Carne A., Bekhit A. A., et al. An improved method for solubilisation of wool keratin using peracetic acid. *Journal of Environmental Chemical Engineering* **5**, 1977-1984, 2017.
17. Hassan M. A., Taha T. H., Hamad G. M., et al. Biochemical characterisation and application of keratinase from Bacillus thuringiensis MT1 to enable valorisation of hair wastes through biosynthesis of vitamin B-complex. *International Journal of Biological Macromolecules* **153**, 561-572, 2020.
18. Rong L., Dong W. Preparation of regenerated wool keratin films from wool keratin-ionic liquid solutions. *Journal of Applied Polymer Science*, 2013.
19. Dąbrowska M., Sommer A., Sinkiewicz I., et al. An optimal designed experiment for the alkaline hydrolysis of feather keratin. *Environmental Science and Pollution Research* **29**, 24145-24154, 2022.
20. Ozaki Y., Takagi Y., Mori H., et al. Porous hydrogel of wool keratin prepared by a novel method: An extraction with guanidine/2-mercaptoethanol solution followed by a dialysis. *Materials Science & Engineering* **42**, 146-154, 2014.
21. Brandelli A. Bacterial keratinases: useful enzymes for bioprocessing agroindustrial wastes and beyond. *Food & Bioprocess Technology* **1**, 105-106, 2008.
22. Mokrejs P., Svoboda P., Hrncirik J., et al. Processing poultry feathers into keratin hydrolysate through alkaline-enzymatic hydrolysis. *Waste Management & Research* **29**, 260-267, 2010.
23. Yan L., Chattha S. A., Zhang X., et al. Effects of Alkali and Acid on the Solubility and Molecular Weight of Collagen Hydrolysates Extracted from Bovine Hide. *JALCA* **117**, 412-422, 2022.
24. Adepoju A. A., Isinkaye O. D., Ofeniforo B. E., et al. Comparative Analysis of Amino Acid Composition in the Head, Muscle and Tail of Fresh African Cat Fish (Clarias gariepinus). *Journal of Agricultural Chemistry and Environment* **11**, 9, 2022.
25. Wongsrangsap N., Chukiatsiri S. Purification and identification of novel antioxidant peptides from enzymatically hydrolysed samia ricini pupae. *Molecules* **26**, 2588, 2021.
26. Matyasovsky J., Sedliacik J., Valachova K., et al. Antioxidant effects of keratin hydrolysates. *JALCA* **112**, 327-337, 2017.
27. Bhushan B. Nanoscale characterization of human hair and hair conditioners. *Progress in Materials Science* **53**, 585-710, 2008.
28. Li J., Li Y., Zhang Y., et al. Toxicity study of isolated polypeptide from wool hydrolysate. *Food and Chemical Toxicology* **57**, 338-345, 2013.

29. Matvay J., Sedliacik J., simon P., et al. Antioxidant Activity of Keratin Hydrolysates Studied by DSCC. *JALCA* **114**, 20-28, 2019.
30. Yao H. L., Yang J., Zhan J., et al. Preparation, amino acid composition, and in Vitro antioxidant activity of okra seed meal protein hydrolysates. *Food Science & Nutrition* **9**, 3059-3070, 2021.
31. Song W., Kong X. Z., Hua Y., et al. Antioxidant and antibacterial activity and in vitro digestion stability of cottonseed protein hydrolysates. *LWT-Food Science and Technology* **118**, 8, 2020.
32. Zheng L., Lin L., Su G., et al. Pitfalls of using 1,1-diphenyl-2-picrylhydrazyl (DPPH) assay to assess the radical scavenging activity of peptides: Its susceptibility to interference and low reactivity towards peptides. *Food Research International* **76**, 359-365, 2015.
33. Sun Q., Zhang X., Gao M. C., et al. Resource utilization of bovine neck ligament: enzymatic preparation of elastin peptide and its antioxidant activity. *Applied Biochemistry and Biotechnology* **195**, 33-50, 2022.
34. Zeng W. C., Zhang W. H., He Q., et al. Purification and characterization of a novel antioxidant peptide from bovine hair hydrolysates. *Process Biochemistry* **50**, 948-954, 2015.

Graphene Oxide Modified Dye: Preparation and its Application in the Dyeing of Biomass-Derived Aldehyde-Tanned Chrome-Free Leather

by

Song Guo,[1,3] Wei Ding,[1,3*] Xiaoyan Pang[1,2] and Zhiwen Ding [1,2*]

[1]*China Leather and Footwear Research Institute Co. Ltd*., Beijing 100015, P.R. China

[2]*Key Laboratory of Leather and Footwear Green Manufacturing Technology of China Light Industry*, Beijing100015, China

[3]*China-Ethiopia Leather Technology 'One Belt and One Road' Joint Laboratory*, Beijing 100015, China

Abstract

In this work, a graphene oxide (GO) modified small molecule reactive dye was prepared and further applied in the dyeing of the biomass-derived aldehyde tanning agent (BAT) tanned chrome-free leather for clarifying its application properties. The modified dye (GORD) was prepared by introducing Reactive Red180 (RRD-180) onto the surface of GO using the dehydration condensation method. GORD was characterized using FTIR spectroscopy, UV-Vis spectroscopy, and thermogravimetric analysis. The uptake ratios and the color fastness to sunlight of the GORDs were tested. FTIR and amino group consumption tests showed that RRD-180 was successfully grafted onto the GO lamellar structure, and the color rendering feature of the GORD was similar to that of RRD-180. The introduction of GO reduced the initial degradation temperature of GORD in the second stage (from 170°C to 150°C), but this did not affect the shrinkage temperature of the dyed leather. The uptake ratios of RRD-180 and GORDs were both higher than 90%, indicating that GO modification did not affect the reactive dye's uptake by leather. Importantly, the coloring fastness to sunlight of the grain and flesh sides of the dyed leather was improved, indicating that the GORD endowed the dyed leather with a certain UV-shielding performance. This work provides new ideas for promoting the industrial applications of GO and GO-based functional materials in chrome-free leather manufacturing.

Introduction

Reactive dyes contain groups that can react with cellulose and protein fibers under suitable conditions to form covalent bonds, thus achieving good fastness properties.[1] However, the light fastness of the products dyed with reactive dyes is relatively poor, especially for light-colored fabrics, which are difficult to meet the requirements of use.[2] Graphene has an ultraviolet absorption peak at approximately 281 nm, so it can absorb ultraviolet light in the wavelength range of 100 nm to 281 nm. For wavelengths greater than 281 nm, the two-dimensional planar structure of graphene can act as an impedance through reflection, thus enhancing the UV aging resistance.[3] Therefore, graphene and its derivatives have been extensively used in the coating of textile materials to obtain functional fabrics with UV-shielding properties. However, graphene is hydrophobic and easy to agglomerate due to strong van der Waals forces, which limits its wide application.[4]

Graphene oxide (GO) is a derivative of graphene, which has good dispersion stability in water and most polar organic solvents.[5] Compared with graphene, GO has excellent properties, which not only includes good wettability and surface activity, but also can be exfoliated by small molecules or polymers after intercalation, and play a very important role in improving the comprehensive performance of materials such as thermal, electrical and mechanical properties.[6,7] Xie et al. reported a facile strategy to prepare functional Poly (vinyl alcohol) (PVA) hybrid film with good ultraviolet (UV) shielding property and visible light transmittance using GO nanosheets as UV-absorbers.[8] The absorbance of ultraviolet light at 300 nm could be up to 97.5%, while the transmittance of visible light at 500 nm remained 40% plus. This hybrid film could protect proteins from UVA light induced photosensitive damage, remarkably. R. Miraftab et al. prepared GO-AZO composites by grafting amino groups on azo dyes with epoxy groups on GO.[9] The GO-AZO/PU composites were blended into a polyurethane matrix under optimal conditions and the GO-AZO/PU composites significantly improved its durability and resistance against degradation when exposed to UV irradiation.

In our previous work, GO was incorporated into waterborne polyurethane-based polymeric dyes to prepare GO modified polymeric dyes.[10] It was found that the introduction of GO into polymer dye systems can improve the heat resistance and sunlight fastness properties of the material. The GO modified waterborne polyurethane-based dye had the potential to be used in high performance leather finishing. Based on this, in this work, a GO modified reactive dye (GORD) was prepared using the carboxyl and epoxy groups on GO and the amino group on Reactive Red-180 through a dehydration condensation reaction. This composite dye was then applied to the dyeing of BAT-tanned chrome-free leather to improve the UV shielding performance of the dyed leather and provide a new idea for industrial applications of GO.

*Corresponding author email: dingwei1368@outlook.com; ding-zhiwen@163.com

Manuscript received February 26, 2023, accepted for publication April 16, 2023.

Experimental

Materials

Graphite powder (2000 mesh) was purchased from Hanhui Graphite Co., Ltd (Shenzhen, China). Sulfuric acid (98 wt%), potassium permanganate, sodium nitrate, hydrogen peroxide, and hydrochloric acid (37 wt%) were bought from Sinopharm Chemical Reagent Co., Ltd (Shanghai, China). Pickled sheepskin was purchased from Xinji Lingjue Leather Co., Ltd (Xinji, Hebei, China). Reactive Red-180 (RRD-180), Potassium iodide starch test paper, were bought from Shanghai Macklin Biochemical Co., Ltd (Shanghai, China). N,N'-dicyclohexylcarbodiimide (DCC) was bought from Woogood Dongfang Co., Ltd (Beijing, China). Hydrochloric acid (37%), potassium bromide, sodium nitrite, N-N-Dimethylacetamide (DMAC) were bought from Shanghai Aladdin Biochemical Technology Co., Ltd (Shanghai, China). Biomass-derived aldehyde tanning agent was prepared according to the method described by Ding et al.[11,12]

Preparation of GORD

GO was prepared using a modified Hummers' method, which was reported in our recent work.[10] Firstly, 1.0 g of graphite, 0.5 g of sodium nitrate, and 8.0 g of potassium permanganate were added to a three-necked flask. Then, 40 mL of concentrated sulfuric acid was slowly added, and the reaction was carried out at a low temperature of 0°C for 5.5 h, followed by a medium-temperature reaction at 35°C for 3.0 h. The reaction temperature was then raised to 95°C, and 40 mL of distilled water was slowly added drop by drop into the three-necked flask and kept warm for another 30 min. Finally, 100 mL of distilled water was added, and hydrogen peroxide was added dropwise until the solution turned bright yellow. The liquid was filtered, and the filtrate was washed with a 5% dilute hydrochloric acid solution, followed by multiple washes with distilled water until the pH of the liquid was neutralized to 6.5~7. The product was then dried at 60°C to obtain graphite oxide.

As the preparation scheme of GO modified Reactive Red-180 (GORD) shown in Figure 1, graphite oxide was firstly added into 100 g of DMAC and dispersed with an ultrasonic disperser (below 20°C, 800 W, 24 min) to obtain a GO dispersion. Then, 20 g of RRD-180 and 5 g of DCC were added to a three-necked flask containing the dispersed GO solution, the mixture was mechanically stirred at 60°C in a thermostatic oil bath for 6 h and stood overnight. It was important to note that the mass of GO used was 0%, 0.1%, 0.4%, 0.7%, and 1.0% of the mass of RRD-180, respectively. The upper clear layer was poured into a glass evaporation vessel and dried in a constant temperature blast oven at 60°C for 24 h. The dried crude product was ground into powdery product using an agate mortar and collected for further use. The products with different GO dosages were defined as GORD-0.1%, GORD-0.4%, GORD-0.7%, and GORD-1.0%, respectively.

Dyeing of leather using GORD

Firstly, the pickled sheepskin was weighed, and the dosage of experimental materials was calculated as 200% of the weight of the pickled sheepskin. The tanning process was carried out in a drum. Pickled sheepskin, 100% of water, and 6% of sodium chloride were added into the drum and rotated for 30 min. After that, 2% of BAT was added to the drum and rotated at room temperature for 4 h. The pH of the tanning liquor was then slowly adjusted to 8.0 using sodium bicarbonate, and the tanning liquor was heated to 40°C. After running for another 4 h, the drum was stopped overnight. Finally, the tanned leather was washed using 400% of water at room temperature for 10 min and then horsed up for 24 h to obtain the BAT-tanned leather.[13,14]

Next, BAT-tanned chrome-free leather was shaved to a thickness of 1.0 mm and weighed. Twice the weight was used as the weight benchmark of the subsequent chemicals. Shaved BAT-tanned leather and 200% of water were added to the drum and ran for 20 min. The pH of the treatment liquor was measured and adjusted to 5.0~5.5 by adding the appropriate amount of formic acid. After running for 40 min, the liquor was drained. Next, 2.0% of GORD and 200% of water were added into the drum, which was then kept running for 2 h at 50°C. Finally, 1.5% of formic acid was added to adjust the pH of the dyeing liquor to 3.8~4.0. After running for 20 min, the dyeing

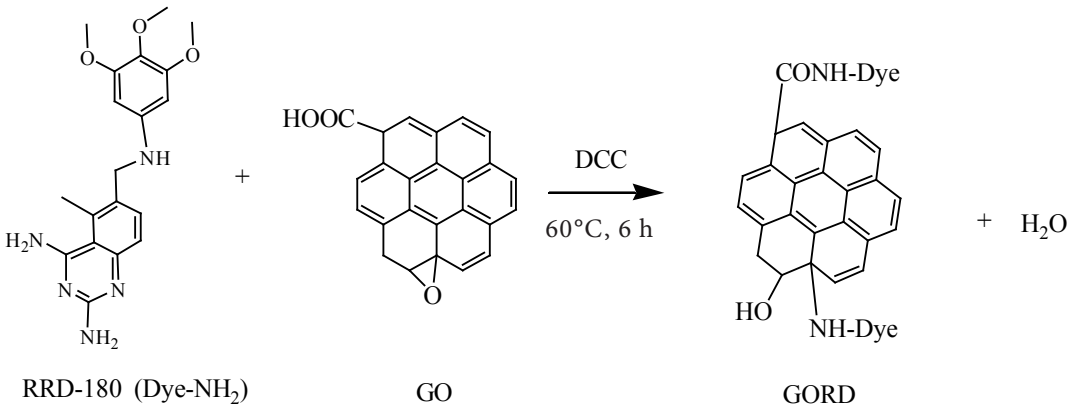

Figure 1. The schematic diagram for the modification reaction between GO and RRD-180.

liquor was drained, and the dyed leather samples were naturally dried for further analyses. The sample dyed with 2.0% of RRD-180 was used as a control group for comparison.

Characterizations

The Fourier transform infrared spectroscopy spectra of dyes were recorded by Tensor 27 infrared spectrometer (Bruker Inc., Billerica, Massachusetts, USA) with the scanning range in the spectrum of 600~4000 cm^{-1}. The UV-vis spectra of the GO, RRD-180, and GORD solutions were recorded by the TU-1810 ultraviolet-visible spectrophotometer (PERSEE, Beijing, China). Thermogravimetric measurements of dyes were performed in a nitrogen atmosphere using a TGA Q500 thermogravimetric analyzer (TA Instruments of America). The samples ranging from 7 mg to 8 mg in weight were heated from 25°C to 800°C at a heating rate of 20°C/min and under a nitrogen flow of 10 mL/min. Shrinkage temperature (T_s) is the most common index used to characterize the hydrothermal stability of leather.[15] Thus, the dyed samples were sampled to test their T_s using a digital leather shrinkage temperature instrument (MSW-YD4, Sunshine Electronic Research Institute of Shaanxi University of Science and Technology, Xi'an, Shanxi, China).

The coloring fastness to sunlight was used to assess the UV-shielding effect of the dyed leather via employing the LY-605A yellowing resistance tester (Dongguan Liyi Experiment Instrument Co., Ltd., Dongguan, Guangdong, China). The testing was conducted according to the GB/T 30669 standard method (340 nm, energy of 0.77 W/(m^2·nm)) at a chamber temperature of 60°C for 24 h. The color change of the leather sample was evaluated using an automatic color difference meter SC-80C (Beijing Kangguang Optical Instrument Co., Ltd., Beijing, China) for the measurement of L* a* b* values both before and after 24 h of irradiation. The color difference ΔE was calculated according to Equation 1.[16]

$$\Delta E = \sqrt{(L_{0h} - L_{24h})^2 + (a_{0h} - a_{24h})^2 + (b_{0h} - b_{24h})^2} \quad (1)$$

The amino group content of GORD was determined by titration using sodium nitrite solution.[14,17] GORD (2.0 g) was added into a volume-metric flask and diluted to 100 mL using distilled water. After that, 10 mL of the aforementioned diluted solution, 100 mL of distilled water, 5 mL of hydrochloric acid, and 5 mL of KBr solution (100 g/L) were added into a beaker. Under constant stirring, sodium nitrite standard solution (1.20×10^{-2} mol/L) was used to titrate the sample at 0~5°C, and a blank sample was tested at the same time. The amino group content (AC wt%) was calculated according to Equation 2.

$$AC\ (wt\%) = c \times (V_1 - V_2) / m \times 16 \times 100\% \quad (2)$$

where 'c' is the concentration of sodium nitrite standard solution (mol/L), V_1 is the consumed volume of sodium nitrite standard solution for sample titration (L), V_2 is the consumed volume of sodium nitrite standard solution for sample blank titration (L), and 'm' is the dry weight of the sample to be tested (g). Similarly, the AC of RRD-180 was determined using the same method. The amino group consumption ratio was calculated according to Equation 3.

$$\text{Amino group consumption ratio } (\%) = 1 - AC_{GORD} / AC_{RRD\text{-}180} \times 100\% \quad (3)$$

Before and after the dyeing processing, the treatment liquor was collected to determine the total organic carbon (TOC) concentration (multi N/C 2100, Analytik Jena, Jena, Thuringia, Germany). The uptake ratio of dye was calculated according to Equation 4.

$$\text{Uptake ratio of dye } (\%) = (C_0 - C_1) / C_0 \times 100\% \quad (4)$$

C_0 is the TOC value of diluted raw filler-dye solution multiplied by the dilution multiple; C_1 is the TOC value of diluted filling-dyeing wastewater multiplied by the dilution multiple.

Statistical analysis

For all experimental analysis at least 3 samples were used. Data for each group were presented as the mean ± SD ($n \geq 3$). Statistical analysis was performed with the software GraphPad Prism 8.0.1 (GraphPad Software, USA) by using ordinary one-way ANOVA method without matching and correction for multiple comparisons. RRD-180 and its dyed leather sample were set as controls. The statistical significance was defined at $p < 0.05$.

Result and Discussion

Structure characterizations

The structures of GO, RRD-180, and GORD-1.0% were characterized by FTIR. As presented in Figure 2, for the spectrum of GO, the strong broad absorption peak at 3200~3700 cm^{-1} was generated by the hydroxyl stretching vibration.[18] The peak at 1730 cm^{-1} was the characteristic peak of carbonyl stretching vibration in the carboxyl group at the edge of graphene oxide,[19] and the peak intensity was weak because the carboxyl group is generally distributed at the edge of graphene oxide with less quantity. The peak at 1635 cm^{-1} was the C=C stretching vibration peak of the graphene oxide benzene ring-like skeleton structure.[20] The absorption peak at 1398 cm^{-1} was the characteristic peak of the stretching vibration of the carboxylic acid C-O at the edge of graphene oxide,[21] and the absorption peak near 1076 $cm^{-1}$was generated by the C-OH stretching vibration of alcohols.[22] Compared to the FTIR spectra of RRD-180, the FTIR spectra of GORD-1.0% showed a much weaker peak for the absorption vibration of -NH_2 at 3448 cm^{-1},[23] a wider and stronger absorption band for the stretching vibration of the C-N bond at 1415 cm^{-1}, and stronger absorption peaks for the amide II band at 1558 cm^{-1} and the amide III band at 1335~1200 cm^{-1}.[24,25] All the above indicated that new amide bonds were formed.

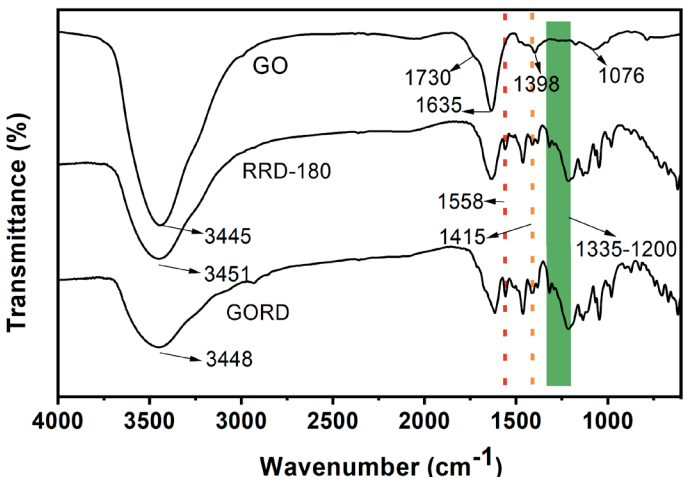

Figure 2. FT-IR spectra of GO, RRD-180, and GORD-1.0%.

UV-vis absorption spectra of GO, RRD-180, and GORD samples in the wavelength range of 200~800 nm were presented in Figure 3. It illustrated that the characteristic absorption peaks of RRD-180 appeared at 515 nm and 540 nm in the visible range, respectively. It could be also observed that the absorption curves of GORD and RRD-180 were very similar. Besides, in the region of 200~400 nm, the absorption curves of GORD and RRD-180 were very similar. The peak of RRD-180 at 540 nm slightly shifted to 539 nm after the modification with GO. This indicated that the color rendering of the dye did not change before and after the modification.

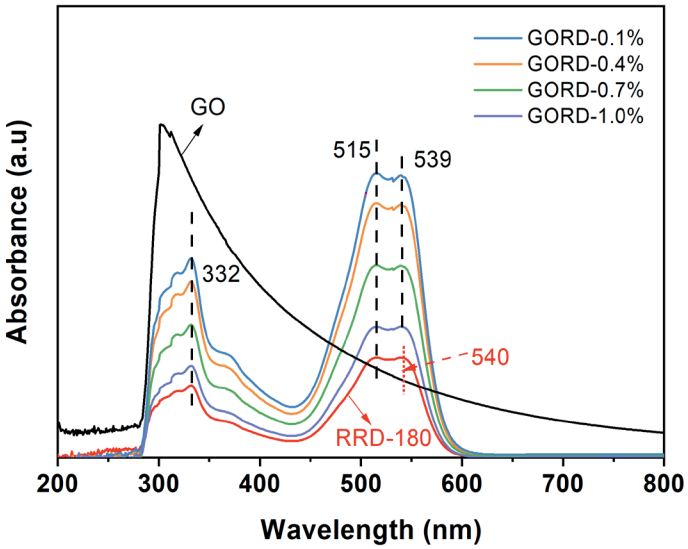

Figure 3. UV-vis spectra of GO, RRD-180, and GORD.

The amino group contents of RRD-180 and GORDs are shown in Table I. The amino group consumption ratio during the reaction can be calculated by detecting the amino group content in the solution before and after the reaction, and the consumption ratios of the amino group were presented in Figure 4. It could be observed that the consumption ratio of the amino group first decreased slightly with the increase of GO, and then increased with the increase of GO dosage after exceeding 0.7%. Overall, the consumption ratio of the amino group was around 50%, which might be due to the fact that there were two amino groups on the RRD-180, and there were fewer carboxyl groups on GO, thus it was more difficult for one amino group on RRD-180 to react with GO. Then, the other amino group was more difficult to contact with the carboxyl groups, so the amino group consumption ratio of the as-prepared GORD was around 50%. According to the significance analysis of the data shown in Table I, it can be determined that the amino group contents of GORDs were significantly different from that of RRD-180, further demonstrating the obvious consumption of amino group from RRD-180 during the preparation process of GORD.

Furthermore, the thermal stability of GORD was investigated via thermogravimetric analysis (TGA). It could be observed that the TGA curves of GO were mainly divided into three stages (Figure 5). The first stage was from 25°C to about 150°C and was mainly caused by the absorption of water by GO, accounting for about 8.9% of the total GO mass. The second stage occurred between 150°~240°C and was mainly caused by the cleavage of unstable oxygen-containing

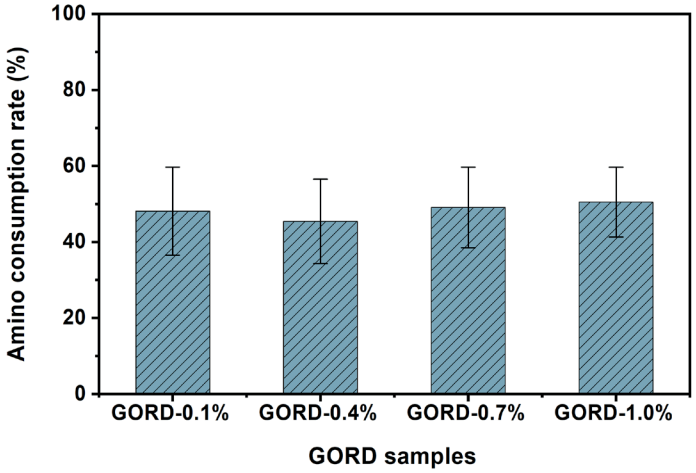

Figure 4. Consumption ratio of the amino group during the synthesis of GORD.

Table I

The content of amino groups in RRD-180 and GORD

Samples	RRD-180	GORD-0.1%*	GORD-0.4%*	GORD-0.7%*	GORD-1.0%*
Content (%)	8.31±0.66	4.31±0.97	4.54±0.93	4.24±0.88	4.12±0.77

The values are represented as mean ± standard deviation. * represents the significant difference ($p < 0.05$), and the RRD-180 sample was used as the control.

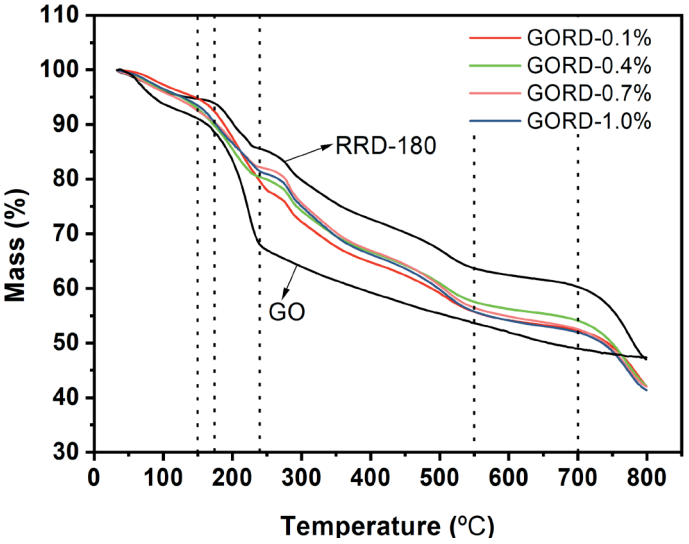

Figure 5. TGA curves of GO, RRD-180, and GORD.

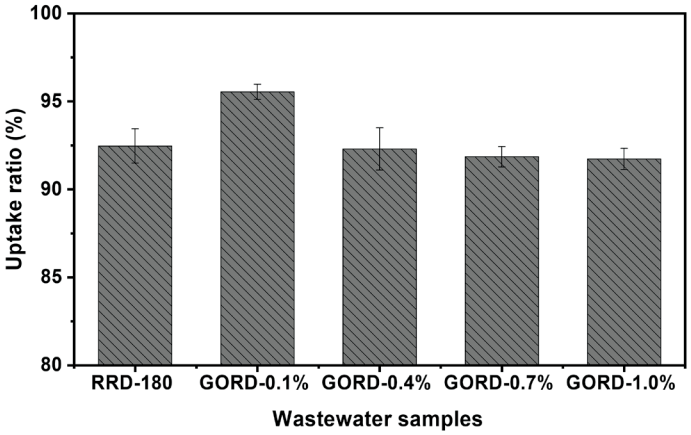

Figure 6. The uptake ratio of RRD-180 and GORD.

functional groups,[26] with a weight loss of about 23.1% at this stage. The third stage occurred after 300°C and was the degradation of more stable oxygen-containing functional groups on GO or the GO backbone.[27] The TGA curves of RRD-180 were mainly divided into four stages: 25°~170°C, 170°~550°C, 550°~700°C, and after 700°C. Impacted by the thermal weight loss of introduced GO, the second stage weight loss temperature of GORD was reduced to about 150°C. Meanwhile, the weight loss rate of GORD was higher in the interval of 170°~240°C compared with that of RRD-180. After 240°C, the thermal weight loss rate of GORD was the same as that of RRD-180.

Application performances of GORD in leather dyeing

The shrinking temperature (T_s) is used to characterize the hydrothermal stability of the leather. The T_s of the dyed leather samples ranged from 70°~71°C (Table II) with no major differences among different leather samples. This suggested that the GORD had no negative effect on the hydrothermal stability of the leather samples, which was probably due to a very small amount of GO used in the dyeing test, at most one part in ten thousand.

The uptake ratio of dye was calculated by measuring the total organic carbon concentration of the dye baths before and after dyeing. The maximum uptake ratio of the dye was achieved at 95.5% when the amount of GO/RRD-180 was 0.1%. Further increasing the dosage of GO, the uptake ratio of the GORD decreased slightly (Figure 6). Nevertheless, both RRD-180 and GORD showed an uptake ratio higher than 90%, indicating that the GORD had a good uptake ratio and the introduction of GO did not negatively affect the penetration and fixation of the modified dye. With the outstanding adsorption and penetrability of RRD-180 and GORDs, they had completely penetrated into the interior of the leather.

The color fastness to sunlight irradiation is an important application performance of dyes and materials. The photofading mechanism of dyes is very complicated, but the main reason is that the dyes are excited after absorbing photons, and a series of photochemical reactions occur to destroy the structure, resulting in discoloration and fading.[28] As shown in Figure 7, the ΔE value of the grain side and flesh side of GORD dyed samples were lower than that of the RRD-180 dyed sample after being irradiated by sunlight under the same conditions. With increasing the additive amount of GO in the GORD, the ΔE value of the flesh side of GORD-dyed leather became lower, and the ΔE value of the grain side of GORD-dyed samples increased slightly, but it was still lower than that of RRD-180 dyed leather sample, indicating that the color change of GORD dyed leather samples under sunlight exposure was weaker. According to the significance analysis results, for the grain side, the color fastness of leather dyed with GORD-0.1% had no significant difference

Table II

The T_s of the dyed leather samples

Samples	RRD-180	GORD-0.1%	GORD-0.4%	GORD-0.7%	GORD-1.0%
T_s/°C	70.7±0.53	70.9±1.64	70.0±0.42	70.3±1.90	71.0±1.15

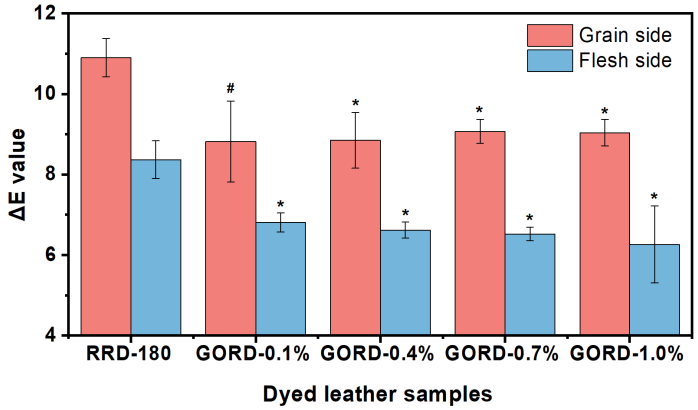

Figure 7. ΔE values of dyed leather samples after being exposed to sunlight for 24 h. The values are represented as mean ± standard deviation. # represents that the data had no significant difference ($p > 0.05$), and * represents the significant difference ($p < 0.05$). RRD-180 dyed leather sample was used as the control.

compared with that of leather dyed with RRD-180. Whereas, the color fastness of leathers dyed with other GORDs had significant difference compared with that of leather dyed with RRD-180. For the flesh side, the color fastness of all the GORDs-dyed leathers had significant difference compared with that of leather dyed with RRD-180. This suggested that the GO, evenly dispersed on the surface of the samples, was capable of improving the color fastness to sunlight of the leather samples. This was because the GO fragments in the GORD had the potential to absorb and reflect some of the neutrons to lower the photons absorbed by dye molecules.[29] As a result, the dyed leather showed better fastness to sunlight. The above results illustrated the success of preparing a composite dye with UV-shielding ability, which improved the color fastness of dyed leather to sunlight.

Conclusions

Graphene oxide modified Reactive Red-180 (GORD) was prepared and used in the dyeing of biomass-derived aldehyde-tanned chrome-free leather in this work. The thermal properties, uptake ratio, shrinkage temperature, and sunlight fastness of GORD with different graphene oxide (GO) contents were investigated. The successful synthesis of GORD was demonstrated using IR analysis, UV analysis, and end-amino content testing. The introduction of GO was found to reduce the heat resistance of the GORD by TGA, due to the presence of more unstable functional groups on the GO. The application experiment suggested that the GO modification did not negatively affect the dye uptake ratio and the shrinkage temperature of dyed leather. Importantly, the sunlight fastness of the GORD-dyed leather was improved, which indicated that the GORD had UV-shielding ability and could improve the weathering performance of the dyed leather. This work further explores the application scope of GO, which is beneficial for the industrialization of GO and GO-based materials.

Acknowledgments

The authors were grateful to the financial supports provided by the National Natural Science Foundation of China (52073301, 22108297), the Beijing Nova Program (Z211100002121085), the National Key Research and Development Program (2020YFE0203800), and the Science and Technology Innovation Key Project of Sinolight Corporation (ZQ2021YY05).

References

1. Siddiqua, U. H., Ali, S., Hussain, T., et al.; Application of Multifunctional Reactive Dyes On the Cotton Fabric and Conditions Optimization by Response Surface Methodology. *J. Nat. Fibers.* **19**, 1094-1106, 2022.
2. Zhao, Z., Zhang, M., Hurren, C., et al.; Effects of Uv Absorbers and Reducing Agents On Light Fastness of Cotton Fabrics Pre-Dyed with Sodium Copper Chlorophyllin and Gardenia Yellow. *Text. Res. J.* **90**, 2245-2257, 2020.
3. Ahmed, A., Adak, B., Bansala, T., et al.; Green Solvent Processed Cellulose/Graphene Oxide Nanocomposite Films with Superior Mechanical, Thermal, and Ultraviolet Shielding Properties. *ACS Appl. Mater. Inter.* **12**, 1687-1697, 2020.
4. Liu, H., Gao, J., Xue, M., et al.; Processing of Graphene for Electrochemical Application: Noncovalently Functionalize Graphene Sheets with Water-Soluble Electroactive Methylene Green. *Langmuir.* **25**, 12006-12010, 2009.
5. Yang, X., Li, Y., Yang, M., et al.; High Performance Leather Based On in Situ Formation of Reduced Graphene Oxide in Chrome Tanning. *JALCA* 117, 206-211, 2022.
6. Dideikin, A. T., Vul', A. Y.; Graphene Oxide and Derivatives: The Place in Graphene Family. *Front. Phys.* **6**, 149, 2019.
7. Zhang, Z., Cui, M., Wang, Z., et al.; Preparation and Characteristics of Graphene-Based Polymeric Leather Fatliquor. *JALCA* **115**, 3346-3373, 2020.
8. Xie, S., Zhao, J., Zhang, B., et al.; Graphene Oxide Transparent Hybrid Film and its Ultraviolet Shielding Property. *ACS Appl. Mater. Inter.* **7**, 17558-17564, 2015.
9. Miraftab, R., Ramezanzadeh, B., Bahlakeh, G., et al.; An Advanced Approach for Fabricating a Reduced Graphene Oxide-Azo Dye/Polyurethane Composite with Enhanced Ultraviolet (Uv) Shielding Properties: Experimental and First-Principles Qm Modeling. *Chem. Eng. J.* **321**, 159-174, 2017.
10. Guo, S., Liu, N., Ding, W., et al.; Graphene Oxide Modified Waterborne Polyurethane-Based Dye with High Color-Fastness Performance. *J. Appl. Polym. Sci.* **138**, 50390, 2021.
11. Ding, W.; Bridging-Induced Densification Strategy Based On Biomass-Derived Aldehyde Tanning Integrated with Terminal Al(Iii) Crosslinking Towards High-Performance Chrome-Free Leather Production. *J. Environ. Manage.* **307**, 114554, 2022.

12. Ding, W., Zhou, J., Zeng, Y., et al.; Preparation of Oxidized Sodium Alginate with Different Molecular Weights and its Application for Crosslinking Collagen Fiber. *Carbohyd. Polym*. **157**, 1650-1656, 2017.
13. Ding, W., Zhang, Y., Li, S., et al.; Novel Biomass-Based Polymeric Dyes: Preparation and Performance Assessment in the Dyeing of Biomass-Derived Aldehyde-Tanned Leather. *Polymers* 15, 2300, 2023.
14. Ding, W., Guo, S., Liu, H., et al.; Synthesis of an Amino-Terminated Waterborne Polyurethane-Based Polymeric Dye for High-Performance Dyeing of Biomass-Derived Aldehyde-Tanned Chrome-Free Leather. *Mater. Today Chem*. **21**, 100508, 2021.
15. Esteban, B., Baquero, G., Cuadros, R., et al.; Proposal and Application of a New Method to Determine Leather Shrinkage Temperature. *Thermochim. Acta*. **698**, 178880, 2021.
16. Amrollahi, S., Ramezanzadeh, B., Yari, H., et al.; Synthesis of Polyaniline-Modified Graphene Oxide for Obtaining a High Performance Epoxy Nanocomposite Film with Excellent Uv Blocking/Anti-Oxidant/ Anti-Corrosion Capabilities. *Compos. Part B: Eng*. **173**, 106804, 2019.
17. Zong, L., Teng, J., Ma, D.; The Detection Method of Primary Amino Content in the Polymethylene Polyphenyl Polyamine. *Polyurethane Ind*. **21**, 41-43, 2006.
18. Zhang, C., Dabbs, D. M., Liu, L., et al.; Combined Effects of Functional Groups, Lattice Defects, and Edges in the Infrared Spectra of Graphene Oxide. *J. Phys. Chem. C*. **119**, 18167-18176, 2015.
19. Aliyev, E., Filiz, V., Khan, M.M., et al.; Structural Characterization of Graphene Oxide: Surface Functional Groups and Fractionated Oxidative Debris. *Nanomaterials* **9**, 1180, 2019.
20. Abdelkhalek, A., El-Latif, M. A., Ibrahim, H., et al.; Controlled Synthesis of Graphene Oxide/Silica Hybrid Nanocomposites for Removal of Aromatic Pollutants in Water. *Sci. Rep.-UK*. **12**, 7060, 2022.
21. Mohamadi, M., Kowsari, E., Haddadi-Asl, V., et al.; Fabrication, Characterization and Electromagnetic Wave Absorption Properties of Covalently Modified Reduced Graphene Oxide Based On Dinuclear Cobalt Complex. Compos. *Part B: Eng*. **162**, 569-579, 2019.
22. Emiru, T. F., Ayele, D. W.; Controlled Synthesis, Characterization and Reduction of Graphene Oxide: A Convenient Method for Large Scale Production. Egypt. *J. Basic Appl. Sci*. **4**, 74-79, 2017.
23. Ferreira, F. V., Brito, F. S., Franceschi, W., et al.; Functionalized Graphene Oxide as Reinforcement in Epoxy Based Nanocomposites. *Surfaces and Interfaces*. **10**, 100-109, 2018.
24. Mallakpour, S., Abdolmaleki, A., Borandeh, S.; Covalently Functionalized Graphene Sheets with Biocompatible Natural Amino Acids. *Appl. Surf. Sci. 307*, 533-542, 2014.
25. Xue, B., Zhu, J., Liu, N., et al.; Facile Functionalization of Graphene Oxide with Ethylenediamine as a Solid Base Catalyst for Knoevenagel Condensation Reaction. *Catal. Commun*. **64**, 105-109, 2015.
26. Farivar, F., Yap, P.L., Karunagaran, R.U., et al.; Thermogravimetric Analysis (TGA) of Graphene Materials: Effect of Particle Size of Graphene, Graphene Oxide and Graphite on Thermal Parameters. *C* **7**, 41, 2021.
27. Sharma, N., Sharma, V., Jain, Y., et al.; Synthesis and Characterization of Graphene Oxide (GO) and Reduced Graphene Oxide (RGO) for Gas Sensing Application. *Macromol. Symp*. **376**, 1700006, 2017.
28. Millington, K. R.; Colorfastness. In Engineering of High-Performance Textiles; Miao, M., Xin, J. H., (eds) The Textile Institute Book Series, Woodhead Publishing: New Delhi, pp. 155-186, 2018.
29. Zhang, X., Song, L., Wang, Z., et al.; Highly Transparent Graphene Oxide/Cellulose Composite Film Bearing Ultraviolet Shielding Property. *Int. J. Biol. Macromol*. **145**, 663-667, 2020.

Investigation of High Penetration and Dispersion of Functional Nanoparticles in Leather

by

Ji-bo Zhou,[1] Nan Sun,[1] Xue-pin Liao[1,2]* and Bi Shi[1,2]

[1]*Department of Biomass and Leather Engineering, Sichuan University,* Chengdu 610065

[2]*National Engineering Research Center of Clean Technology in Leather Industry,* Chengdu 610065

Abstract

The use of nanoparticle-based functional leather products has stimulated sustainable growth of the conventional leather industry. However, functional nanoparticles (FNPs) face challenges to be well penetrated and dispersed in leather because of their aggregation and mismatch charges with leather. In this study, the acrylic resin (AR) retanning agent, which was originally utilized in leather processing, was applied for the modification of FNPs. It has been demonstrated that AR can improve the electrostatic and steric repulsion among nanoparticles, inhibiting their aggregation and ensuring their penetration and dispersion in leather. Because of the limitation of leather porosity, the maximum loading amount for FNPs was about 40wt% (based on leather weight). The leather got higher results in fullness, thickening ratio, and tensile strength when the loading amount of FNPs was 11.25%. Moreover, the proposed approach in this study can be used well for other types of FNPs loaded in leather, suggesting its broad applicability.

Introduction

With the incorporation of functional nanoparticles (FNPs), conventional leather has recently demonstrated great potential in various high-end applications such as ultraviolet blocking, electromagnetic shielding, and *X*-ray shielding.[1-2] The development of these functional leather materials not only increases the value-added of natural leather but also promotes sustainable growth of the conventional leather industry.[3] However, there are also troublesome issues that must be resolved in this process. For example, the effective penetration and dispersion of FNPs into leather is a prerequisite for fabricating advanced functional leather, but FNPs tend to congregate as a result of their heightened van der Waals attractive forces (Figure 1a). The agglomerated FNPs exhibit very large size, and therefore hindering their penetration in leather.[4] Moreover, there are many surface charges present on nanoparticles. As leather making is a well-known charge-related process,[5] the mismatch of surface charges between FNPs and leather further inhibits their penetration and dispersion process.

There are primarily two methods to prevent the agglomeration of FNPs: electrostatic modification and steric repulsion (Figures 1b and 1c).[6] Electrostatic modification involves the adsorption of charged stabilizer molecules on the surface of FNPs, which creates an electrical double layer that facilitates the electrostatic repulsion, thereby restraining aggregation and adjusts the charge on the surface of FNPs.[7] Steric repulsion involves using polymers to increase the steric repulsion among FNPs, thereby inhibiting the aggregation of FNPs.[8] Currently, the steric repulsion method is mainly achieved by surfactants comprising a hydrophilic head group and a hydrocarbon chain (hydrophobic group).[9] The hydrophobic segments of surfactants form a physical barrier on the surface of NPs via hydrophobic interactions, while hydrophilic segments increase the stability of FNPs in suspensions such as water and ethyl alcohol. Based on the above two methods, several chemicals such as polyionic liquids, chitosan, hydrogenated castor oil, and polyethylene glycol have all been attempted as modifications to facilitate the penetration and dispersion of FNPs in leather.[10-13] These agents are effective in specific conditions, but they usually suffer a long time of reaction, multiple steps, cost-prohibitive and the use of more hazardous chemical agents.[14] Besides, the introduction of these chemicals may reduce the comprehensive performances of leather, such as wearing comfort and mechanical strength. Therefore, there is a great demand to develop a novel approach to realize the effective penetration and dispersion of FNPs in the leather.

Looking across the leather-making process, acrylic resin (AR) used in the leather retanning process may offer a solution to the FNPs aggregation issue. In general, AR is a polymer synthesized through the free radical co-polymerization of vinyl monomers, and it has been widely used as a retanning agent in the leather industry due to its excellent filling property.[15] To achieve a better filling performance, AR used in the leather retanning process is usually composed of monomers with hydrophilic groups (-COOH, $-NH_2$) and hydrophobic groups (long-chain acrylates), endowing it the capacity to stabilize FNPs via steric stabilization. Furthermore, AR typically shows negative charges because of the presence of abundant carboxyl groups in its structure, which may increase the

*Corresponding author email: xpliao@scu.edu.cn

Manuscript received March 30, 3023, accepted for publication May 7, 2023.

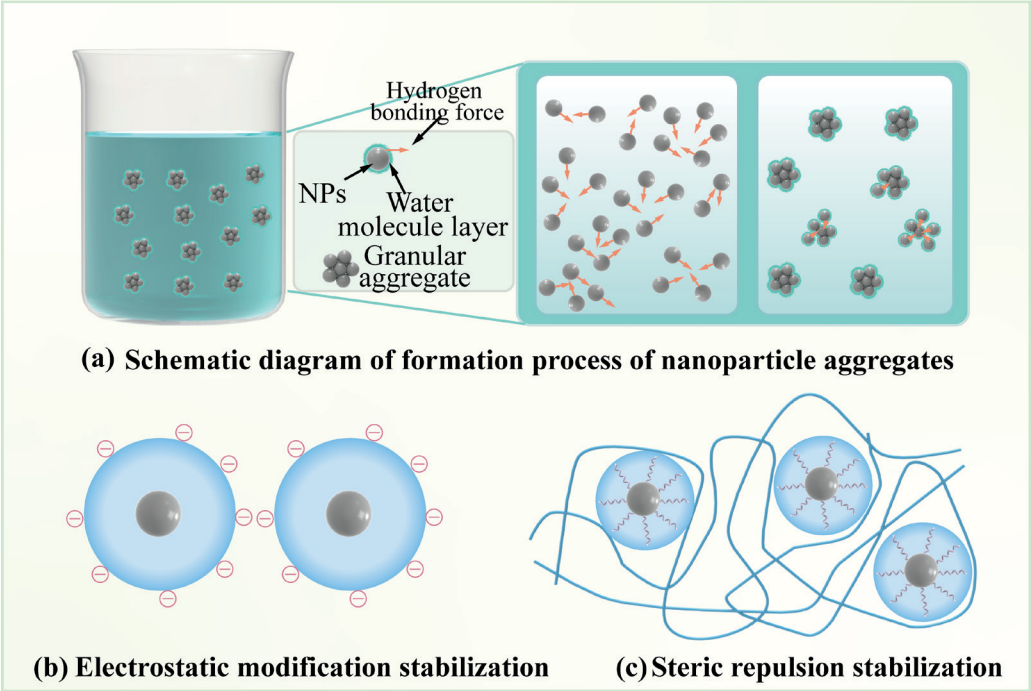

Figure 1. **(a)** Schematic of the aggregation of FNPs. FNPs stabilized by electrostatic modification **(b)** and steric repulsion **(c)**.

electrostatic repulsion between FNPs and inhibit their aggregation. By the synergistic of steric stabilization and electrostatic modification, it is believed that AR would effectively promote the penetration and dispersion of FNPs in leather. Moreover, as AR is a commonly used agent in leather processing, there are no concerns over increased costs and decreased performance of leather. To our knowledge, no studies have yet investigated the effects of AR on the penetration and dispersion of FNPs in leather.

In this study, a novel approach was developed to realize the good penetration and dispersion of FNPs in leather using AR as a modifier. Specifically, gadolinium oxide (Gd_2O_3) nanoparticles (generally used as a functional component of neutron absorption and attenuation of *X*-rays) were considered as representative and the surface morphology of modified Gd_2O_3 FNPs as well as their dispersity and charge properties in water were completely characterized to clarify their penetration and dispersion mechanism in leather. Beyond that, the influence of FNPs on the performance of functional leather was also presented. In addition, the FNPs of B_4C and Bi_2O_3 were also tested to verify the universality of this approach.

Materials and Methods

Materials

Gd_2O_3, B_4C, and Bi_2O_3 nanoparticles (99.9%, 500 nm) used in this study were all obtained from Guangzhou Nano Chemical Technology Co., Ltd. The chrome-tanned and vegetable-tanned leather (both shaved to 1.2 mm) were provided by the National Engineering Laboratory for Clean Technology of Leather Manufacture at Sichuan University. A commercial AR (copolymerized by acrylic acid and long-chain vinyl ester monomers, about 33 wt%) was purchased from Sichuan Decision New Material Technology Co., Ltd. (China). All other chemicals were of analytical grade and purchased from Chengdu Kelong Chemical Co., Ltd.

Modification of FNPs

First, AR was dissolved in water to form a 1:1 (w/w) solution, then Gd_2O_3 FNPs were added to the solution and dispersed by ultrasonication for 30 min at room temperature, and the suspension was stirred at 80°C for 2 h to complete the modification. Finally, the modified Gd_2O_3 was collected and dried in a vacuum at 80°C for 2 h before being used. B_4C and Bi_2O_3 nanoparticles were similarly modified using the same manner.

Physicochemical properties of modified FNPs

FTIR spectra of the pristine and modified Gd_2O_3 nanoparticles were recorded using a Fourier transform infrared spectrometer (Nicolet IS10, Thermo Scientific, USA). X-ray photoelectron spectroscopy (XPS) measurements were conducted using an Escalab Xi+ (Thermo Fisher, USA).

To evaluate the dispersibility and stability of the pristine and modified Gd_2O_3 nanoparticles, they were separately dispersed in deionized water at 0.4 mg/mL and left undisturbed at room temperature for

different times to obtain Gd_2O_3 fluids. The absorbance of FNPs fluids was determined using a spectrophotometer (PerkinElmer, Japan). The size and zeta potential of pristine and modified Gd_2O_3 nanoparticles (in water) were tested using NanoBrook Omni (Brookhaven, USA).

To observe the dispersion of FNPs in the leather matrix, SEM (Nova NanoSEM450, FEI, USA) was used to capture the cross-section of the composites. The composition analysis was performed using energy-dispersive X-ray spectroscopy (EDS, Azteclive Ultim Max 100, Oxford Instruments, UK). The loading amounts of FNPs were determined through ICP-OES after digestion.

Penetration of modified FNPs in leather

Modified FNPs were introduced into the leather matrix using a typical retanning process summarized in Table I.

Effect of different factors on the penetration of FNPs in leather

The effect of different factors on the loading amounts of FNPs, including the amounts of FNPs, pH of bath solution, and water washing, were completely investigated. In particular, to assess the changes of FNPs amount in the leather matrix over pH, the pH of the bath solution was adjusted using different amounts of sodium bicarbonate and formic acid after retanning by modified FNPs via the process shown in Table I, and the leather samples were then treated in the bath for another 2 h before fatliquoring. Furthermore, the water-washing resistance of samples before and after fatliquoring was assessed, with each water-washing cycle of 1 h.

Influence of FNPs on the mechanical performance of leather

All samples were maintained at a temperature of 25° ± 2°C and a relative humidity of 65% ± 2% for over 48 h before measuring. Using a dial thickness gauge (MingYu, China), the average thickness of leather samples was measured, and the thickening ratio (R) was calculated using the formula:

$$R = \frac{(S_2 - S_1)}{S_1} \times 100\%$$

where S_1 and S_2 are the average thicknesses of leather samples before and after retanning with FNPs, respectively.

The physical and mechanical properties of samples, such as tensile strength, and tearing strength, were evaluated using an ISO 3377-2:2016 and ISO 3376:2020 compliant universal testing machine (GOTECH, China). The micropore structures of composites were analyzed using a mercury intrusion porosimeter (Micromeritics, USA).

Table I
Retanning Processes

Process	Chemicals	Dosage %	Temperature (%)	Duration (min)	Remarks
Rewetting	Water	250	40		
	Degreasing agent	0.3			
	Formic acid	0.5		60	pH≈3.2, Drain
Washing	Water	400		10	Drain
Neutralization	Water	200	35		
	Sodium formate	2		30	
	Neutralization tannins	2			
	Sodium bicarbonate	1		60	pH≈5.5, Drain
Washing	Water	400		10×2	Drain
Retanning	Water	100	35		
	FNPs	10/20/30/40/60		90	
Fatliquoring	Water	100	50		
	SO	8		50	
	Formic acid	2		4×15	pH≈3.4
Washing	Water	400		10×3	Drain
Note: based on wet blue weight (w/w)					

Results and Discussion

Basic properties of modified FNPs

Figure 2a shows the modification process of Gd_2O_3 FNPs by AR. AR, a commonly used polymer in the leather retanning process, has numerous hydrophobic bonds that facilitate its combination with Gd_2O_3 FNPs via hydrophobic interactions.[16] After modification, a physical barrier was generated on the surface of FNPs, exposing the hydrophilic groups of AR to aqueous environment, as well as leads to additional stabilization via short-range repulsive hydration forces and enhances their steric stabilization. Furthermore, the electronegative carboxyl groups in the molecule of AR can promote electrostatic repulsion among nanoparticles, further enhancing their dispersion stabilities.

To determine the surface structure of the modified Gd_2O_3 FNPs, FTIR analysis was conducted and is shown in Figure 2b. The characteristic peak at 543 cm^{-1} in the spectra of pristine Gd_2O_3 FNPs corresponded to the vibration absorption of the Gd–O–Gd bonds in Gd_2O_3.[17] The broad absorption peak observed at 3463 cm^{-1} corresponded to the O–H absorption band, and it was attributed to the stretching vibration of adsorbed water molecules on the surface of Gd_2O_3.[18] Owing to the atmospheric water and CO_2 molecules, two peaks at 1389 and 1500 cm^{-1} were observed, and they correspond to O–H and C–O stretching, respectively.[19] For the modified Gd_2O_3, a new peak at 1557 cm^{-1} was observed, which is also seen in the AR spectra. This peak was assigned to the vibration of -COOH, indicating the successful adherence of -COOH onto the surface of Gd_2O_3.[20] The new peaks detected at 2948 and 1416 cm^{-1}, which were attributed to $-CH_2-$ in the long chains of AR, further enhanced the modification.[21] AR contains long hydrophobic tails, and the hydrophobic interaction between AR and Gd_2O_3 allows the hydrophobic tails to drain onto the cluster surface, which facilitates the adsorption of AR molecules on the surface of Gd_2O_3 nanoparticles.

The modification process of Gd_2O_3 FNPs can then be confirmed by XPS analysis. As shown in Figure 2c, the XPS survey spectra of pristine Gd_2O_3 primarily demonstrate two distinct peaks at 142.82 and 531.25 eV, which correspond to Gd 4d and O1s, respectively.[22] However, after modification by AR, the relative intensity of Gd 4d considerably decreased, while C1s increased, indicating successful adherence of AR on the surface of Gd_2O_3 nanoparticles. This conclusion is supported by the proportion of each element revealed by XPS (Figure 2d), which shows a decrease in the fraction of the Gd element from 14.77% to 1.80% and an increase in C from 19.47% to 66.33% after modification. Furthermore, Figure 2e shows that the O 1s curves of pristine Gd_2O_3 could be fitted into two peaks at 531.24 and 528.61 eV, assigned to the Gd–O and O–H bonds, respectively.[23]

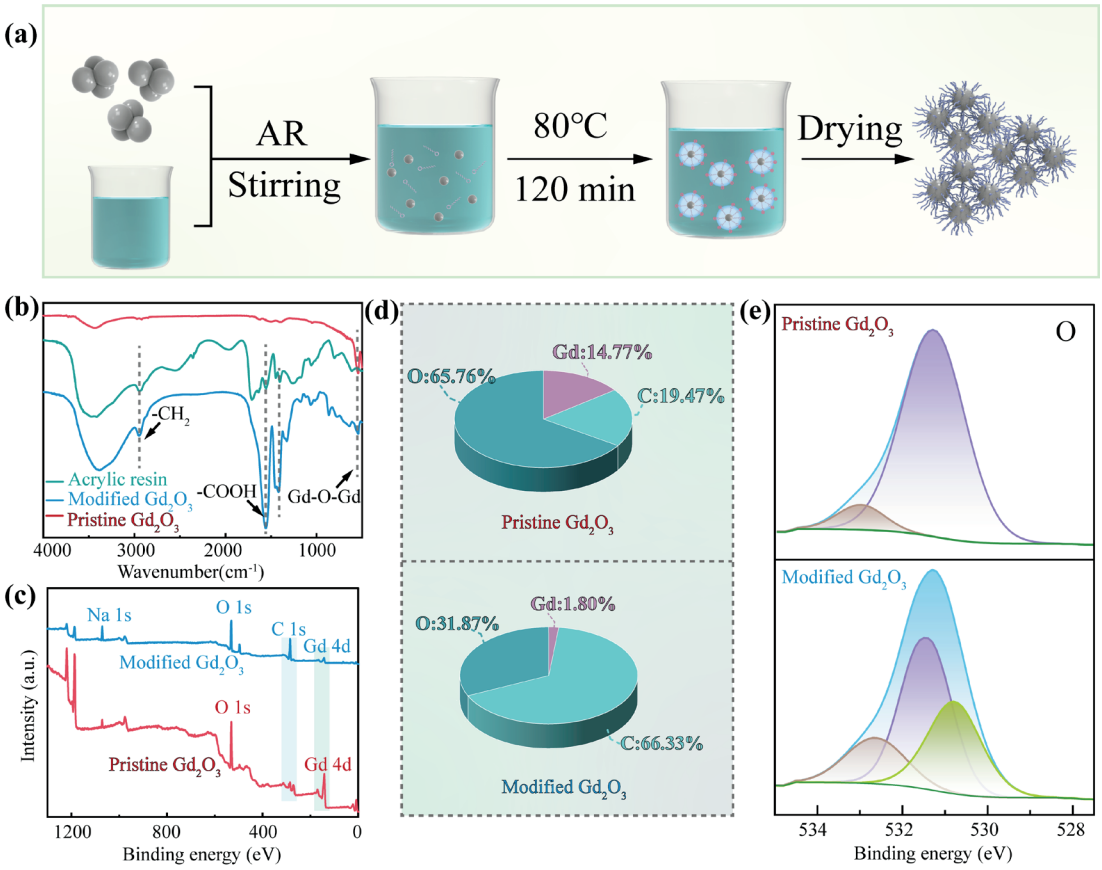

Figure 2. **(a)** Modification process of Gd_2O_3 FNPs by AR, **(b)** FTIR of pristine and modified Gd_2O_3 FNPs, **(c)** High-resolution XPS spectrum of the full spectrum, **(d)** Proportion of elements, and **(e)** O 1s revealed by XPS.

After being modified by AR, a new peak assigned to C=O, can be observed at 530.78 eV; this peak was raised from AR, further confirming the success of the modification.[24]

Analysis of the dispersibility of modified Gd_2O_3 FNPs in water

Leather-making processes are mostly applied in an aqueous environment, where FNPs are more prone to agglomerate because of surface forces such as Van der Waals and electrostatic forces, forming a secondary agglomeration structure that hinders the penetration of FNPs in the leather matrix.[25] Therefore, investigating the dispersion ability of FNPs in water is important to understand their penetration and dispersion process in leather.

In this study, the dispersion stabilities of pristine and modified Gd_2O_3 FNPs in water were examined using a settlement test. As shown in Figure 3a, pristine Gd_2O_3 FNPs were exceedingly unstable because of their large surface area and strong Van Der Waals interaction, resulting in rapid agglomeration and settling at the bottom of the bottle. However, the Gd_2O_3 FNPs modified with AR demonstrated considerably improved dispersion stability under the same condition. The long-chain vinyl ester in the AR molecule lies the foundation for the combination between AR and Gd_2O_3 FNPs via hydrophobic interaction, forming a physical barrier on the surface of FNPs and enhancing its steric stabilization. Furthermore, the charged carboxyl groups in AR can enhance the electrostatic repulsion between nanoparticles and inhibit their aggregation. The synergistic effect of steric stabilization and electrostatic modification largely enhanced the stability of FNPs in water.

According to the literature, only individual FNP exhibit characteristic bands in the UV-vis region, whereas agglomerated FNPs are inactive.[26] As shown in Figure 3b, pristine FNPs exhibit weak absorbance in the wavelength range from 200 nm to 800 nm, with absorbance decreasing as wavelength increases. However, after modification, the absorbance of modified Gd_2O_3 FNPs is higher than that of pristine FNPs, indicating the presence of a certain amount of individually dispersed Gd_2O_3 FNPs in dispersions. This finding is consistent with the settlement investigation, which further demonstrates that AR can effectively inhibit the aggregation of FNPs and improve their dispersibility in water.

The size and electrostatic properties of FNPs are crucial factors that affect their penetration and dispersion in NL. The particle size and zeta potential of the FNPs were therefore determined in this study, and the results are shown in Figures 3c-d. Pristine Gd_2O_3 FNPs (500 nm) exhibited agglomeration in water, resulting in a large particle size of 1632.22 nm, which may impede their penetration into leather The large particle size of FNPs may hinder their penetration in leather. However, after modification with AR, the particle size of modified FNPs decreased to 714.36 nm, showing the effectiveness of AR in preventing the FNPs agglomeration and facilitating their penetration and dispersion in leather. Furthermore, the zeta potential of modified Gd_2O_3 FNPs at different pH was mostly negative because of the increase of electrostatic repulsion caused by the introduction of abundant carboxy groups, remarkably lower than that of pristine Gd_2O_3 FNPs (Figure 3d).[27] As chrome-tanned leather is considered electropositive in the retanning process, the electrostatic attraction between modified Gd_2O_3 FNPs and leather can provide a driving force for the penetration of FNPs in leather. Furthermore, the carboxyl groups on the surface of modified Gd_2O_3 FNPs can coordinate with Cr^{3+}, which is favorable for combining Gd_2O_3 FNPs with leather.

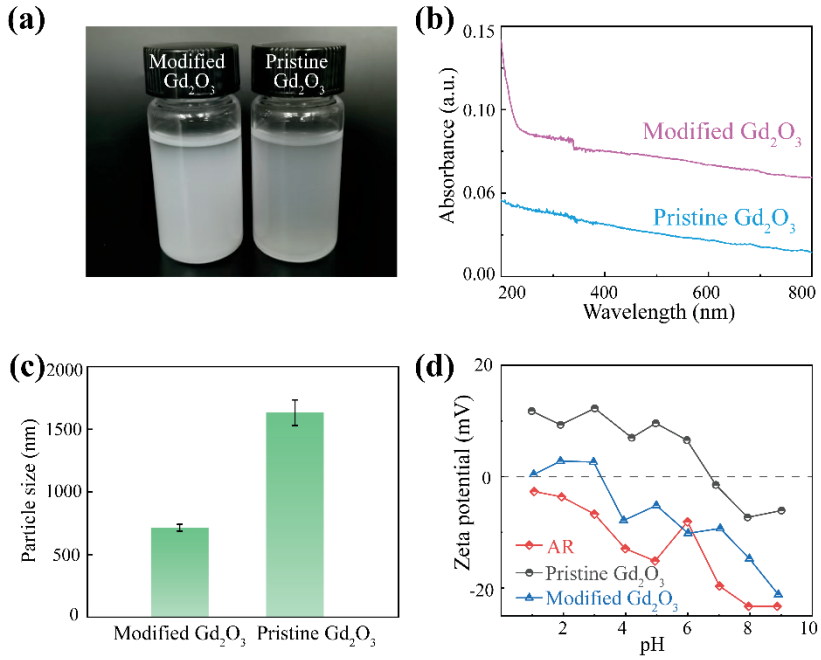

Figure 3. **(a)** Images of pristine and modified Gd_2O_3 FNPs in deionized water. UV-vis **(b)**, particle size **(c)**, and zeta potential **(d)** of pristine and modified Gd_2O_3 FNPs in deionized water.

The aforementioned results have confirmed the successful attachment of carboxyl groups on the surface of Gd_2O_3 FNPs, resulting in modified Gd_2O_3 FNPs with electronegative properties and smaller particle size in water due to their electrostatic and steric repulsion. On the one hand, AR modification improves the electrostatic and steric repulsion among nanoparticles, inhibits the formation of large agglomerations, and ensures the penetration of Gd_2O_3 FNPs in leather. On the other hand, the modified Gd_2O_3 FNPs reveal strong electrostatic interactions with the electropositive leather, which undoubtedly provide a powerful driving force for their penetration into leather.

Penetration of pristine/modified FNPs in leather

To investigate the penetration of modified Gd_2O_3 FNPs in leather, cross-sectional SEM observation of retanned leather were conducted. As shown in Figure 4a, due to the large average particle size resulting from agglomeration and the charge mismatch between FNPs and leather, pristine FNPs struggled to penetrate leather, leading to significant non-uniformity of Gd elements near the grain layer. However, after modification with AR, uniform dispersion of Gd elements was observed (Figure 4b), indicating the successful penetration of modified FNPs in the leather.

Figure 4c summarizes the penetration of pristine and modified Gd_2O_3 FNPs in leather. Commonly, leather making is the penetration and combination of chemical substances in leather, and these two processes are fully affected by the particle size and surface charge of chemicals. On the one hand, AR can effectively form physical barriers on the surface of FNPs with its surface activity, inhibiting the aggregation of FNPs and favoring the penetration of FNPs. On the other hand, the charged groups within the structure of AR can tune the surface charge of FNPs, further enhancing their penetration and dispersion in leather. Overall, the combined effect of these factors facilitates the uniform penetration and dispersion of modified FNPs in leather.

Effect of different factors on the penetration and dispersion of modified FNPs in leather

To further understand the penetration and dispersion of FNPs in leather, various conditions were investigated with loading amounts of FNPs as the index. First, the variation of the loading amounts with the usage of FNPs is shown in Figure 5a. As shown, the loading amounts of FNPs were increased with the increasing dosage of FNPs and gradually attained a plateau. Structurally, leather possesses a sophisticated hierarchical structure from the nanoscale to the macroscale, and the space ranges from micrometers to millimeters among collagen fibers of leather laying solid foundations for the penetration of nanoparticles into the hierarchical network of leather.[28] Although chromed-tanned leather exhibit a high porosity, it is still limited.[29] So, the loading amount of FNPs is saturated as further increasing its dosage.

The effect of pH on FNPs loading amounts was investigated by adjusting the bath pH using formic acid and sodium bicarbonate. Figures 5b-c show that decreasing pH resulted in an increased loading amount of FNPs, indicating the significant influence of surface charge on the penetration of FNPs in leather. The electrostatic attraction between leather and negatively charged modified FNPs was improved when the electropositive property of chrome-tanned leather increased due to the decreased pH of

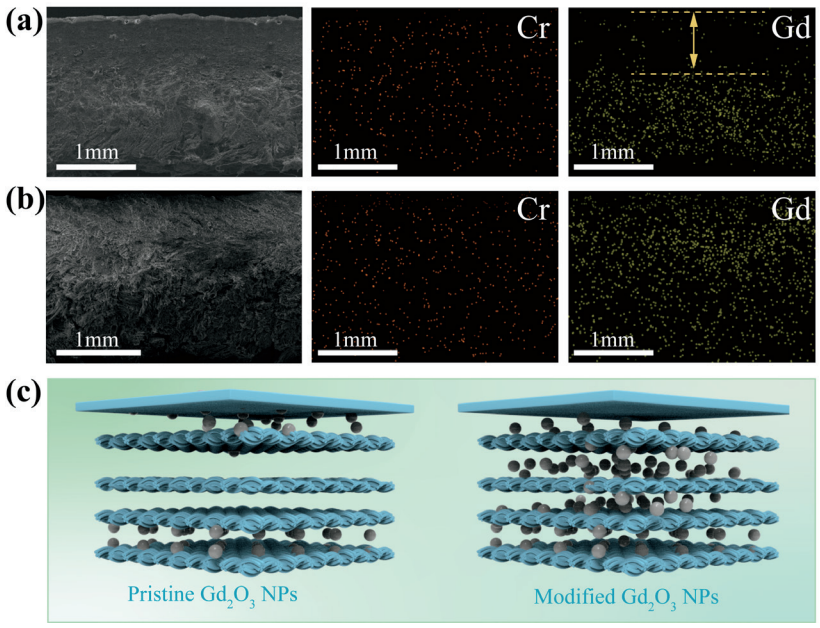

Figure 4. SEM observation of the cross-session of leather retanned with pristine **(a)** and modified **(b)** Gd_2O_3 FNPs. **(c)** Schematic diagram illustrates the penetration of pristine and modified Gd_2O_3 FNPs in leather.

the bath solution. By decreasing the pH of the bath solution, the electropositive property of chrome-tanned leather increased, and the electrostatic attraction between leather and negatively charged modified FNPs was improved.[30] Owing to the enhanced driving force, the penetration of FNPs in leather is much easier. On the contrary, the positive charge of leather was decreased by the increased pH, and the electrostatic attraction between leather and FNPs was weakened, resulting in the lower absorption of FNPs. This result shows that the penetration of FNPs in leather was substantially associated with surface charge, and AR modification can effectively improve the penetration and dispersion of FNPs in leather.

The binding force between FNPs and leather was assessed by investigating the water-washing resistance of prepared composites. Figure 5d shows that the loading amounts of Gd_2O_3 decreased with increased time of water washing cycles, indicating that the combination between FNPs and leather is not strong enough and can be broken by mechanical force. However, after fatliquoring, as the increased times of water washing cycles, the decreasing trend on the loading amounts of FNPs were significantly weakened and it only presented a reduction of 0.03% after three times of water washing. This phenomenon can be assigned to the reason that the fatliquoring process improved the hydrophobicity of the leather, enhancing the hydrophobic interaction between FNPs and leather, therefore enhancing their combination.[31]

Influence of modified FNPs on the organoleptic and physical performance of leather

The organoleptic properties and physical strength characteristics of composites play a key precondition in ensuring the wear comfort of functional leather. To comprehensively investigate the influence of FNPs on the organoleptic properties of leather, the porosity, fullness, thickening ratio, and mechanical performance of leather samples with different amounts of Gd_2O_3 FNPs were all investigated. From Figure 6a, the porosity of the blank leather sample was 64.75%. Because of the filling of Gd_2O_3 FNPs, the porosity of composites sharply decreased, and it was only 46.09% when the loading amounts of Gd_2O_3 FNPs was 39.64%.

The compression-resilience performances of composites are presented in Figure 6b-c. Generally, a higher compressed and resilient thickness implies a better fullness of leather. It can be seen that the leather sample got the best fullness performance when the loading amount of Gd_2O_3 FNPs was 11.25%, and it decreased with a further increase of Gd_2O_3 FNPs amounts, indicating that too high loads of FNPs may decrease the performance of leather. This conclusion can also be supported by the changes in thickening ratio (Figure 6d), where samples got higher results when the loading amount of Gd_2O_3 FNPs was 11.25% and 19.40%, while it decreased as the loading amount of Gd_2O_3 FNPs further increased. Moreover, because of the filling of Gd_2O_3 FNPs, the compressibility of composites all decreased (Figure 6e), but they are mostly more than 5.0 mm, which will not significantly influence their wearable performance. Besides, the density of leather improved obviously due

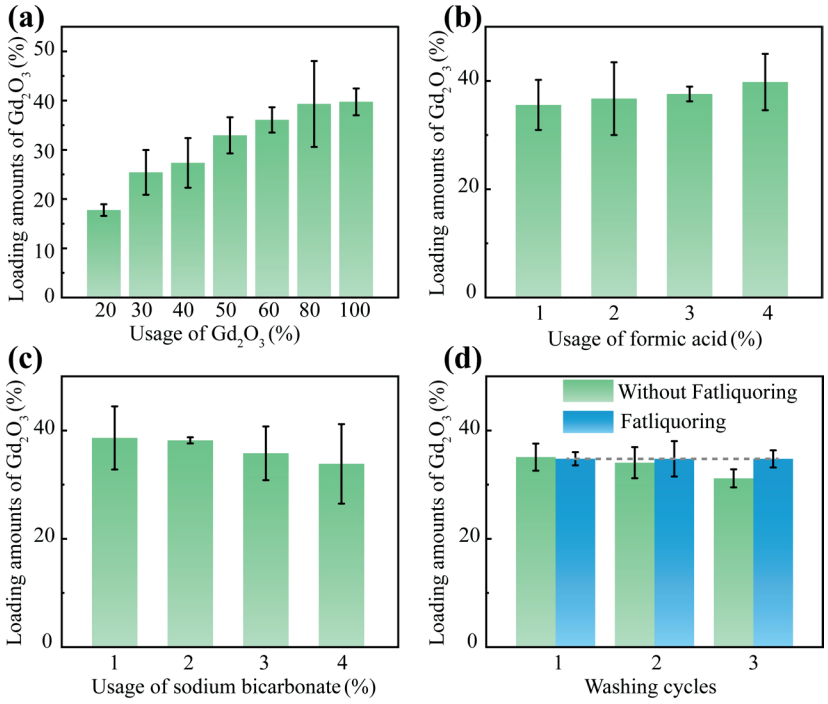

Figure 5. Influence of FNPs usage **(a)**, acid **(b)**, alkaline **(c)**, and washing **(d)** on the loading amounts of Gd_2O_3 FNPs.

to the introduction of Gd_2O_3 FNPs (Figure 6f). From Figures 6g-h, the tensile and tear strength of samples all exhibited a noticeable increase, possibly because of the interaction between FNPs and collagen fiber. More importantly, the shielding efficiency of composites for *X*-rays at 48.3 KeV was investigated when the usage of Gd_2O_3 FNPs was 20%, and the results were shown in Figure 6i. Due to the better penetration and dispersion of FNPs, the modified Gd_2O_3-leather composites get a higher performance, which was 37.94% higher than that of pristine Gd_2O_3-leather composites, demonstrating the necessity of modification in elevating the performance of functional leather.

To determine the universality of the proposed AR modification method, the penetration of B_4C FNPs (500 nm) in chrome-tanned leather and Bi_2O_3 nanoparticles (500 nm) in vegetable-tanned leather were also investigated. Because B_4C is dark black and Bi_2O_3 FNPs are yellow, their penetration in leather can be easily reflected by the color changes on the cross-sections of retanned leathers. As shown in Figure 7a and 7c, it can be observed that the color of cross-section of leather retanned by pristine B_4C/Bi_2O_3 was uneven, implying the difficulty of FNPs in penetration. After being modified by AR, FNPs are well dispersed in leather (Figures 7b and 7d), indicating that the AR modification method fits well with different FNPs.

Conclusion

In this study, a new method was developed for achieving effective penetration and dispersion of FNPs in leather. This was achieved by utilizing acrylic resin as a modifier, which enhances the electrostatic and steric repulsion among nanoparticles, therefore inhibiting their aggregation and ensuring their penetration and dispersion in

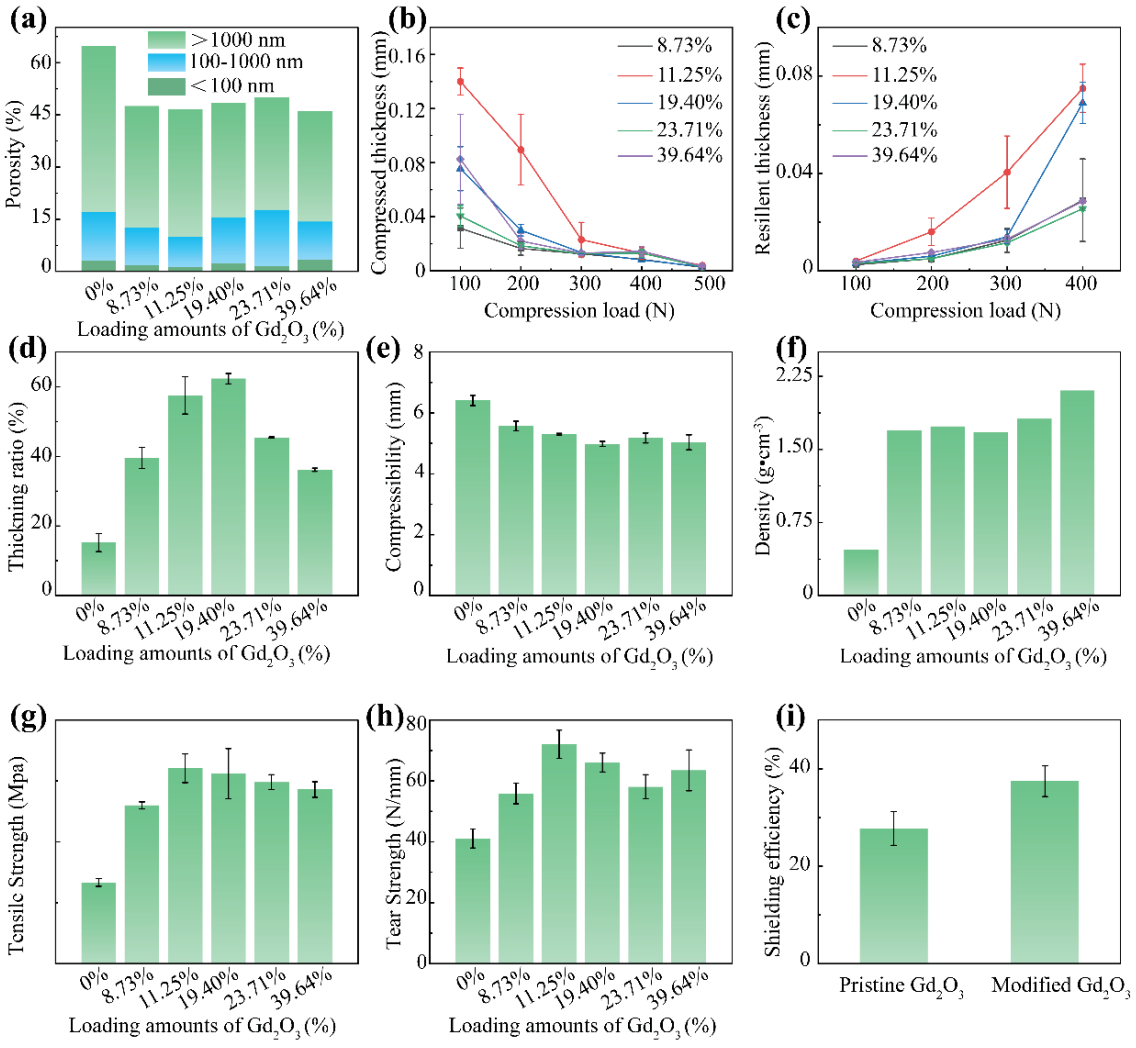

Figure 6. **(a)** Porosity, **(b)** compression, **(c)** resilience, **(d)** thickening ratio, **(e)** compressibility, **(f)** density, **(g)** tensile strength, **(h)** tear strength of different composites, and **(i)** *X*-rays shielding efficiency of different composites.

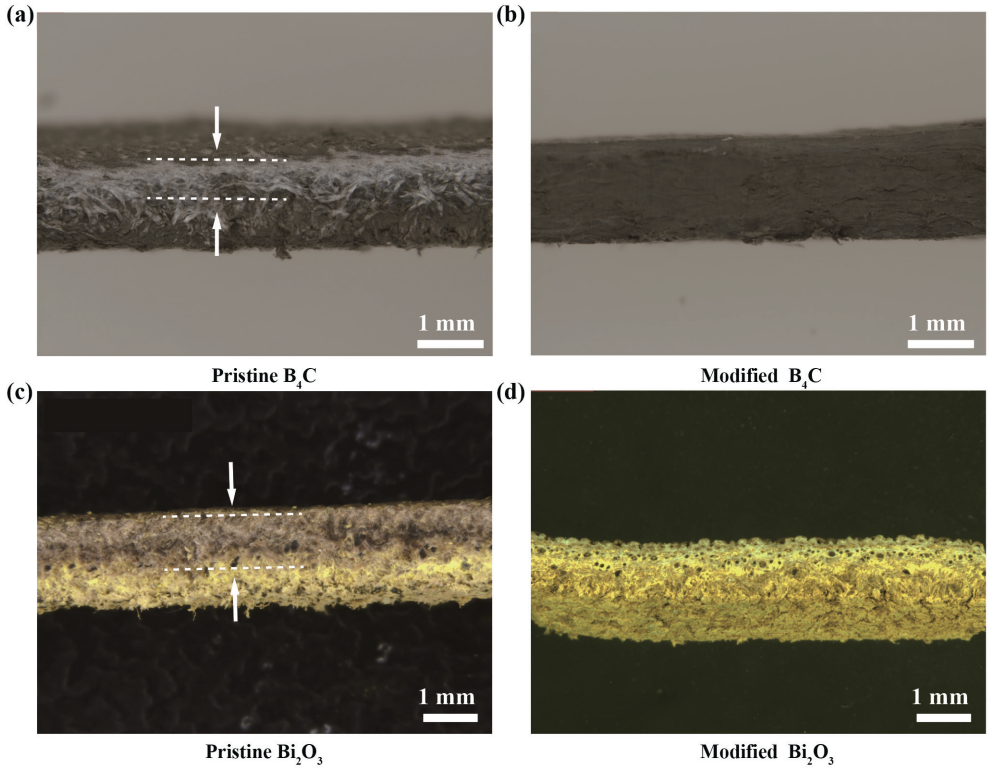

Figure 7. Microscopic pictures of the cross sections of chrome-tanned leather retanned with pristine **(a)** and modified **(b)** B_4C FNPs, and vegetable-tanned leather retanned with pristine **(c)** and modified **(d)** Bi_2O_3 FNPs.

leather. Furthermore, the increase in the leather's electropositivity and hydrophobicity can promote FNP penetration. However, too high loads of FNPs may decrease the performance of composites. The novel acrylic resin-modified approach presented in this study could be applied to other FNPs, offering a useful strategy for the production of nanoparticle-based functional leather.

Acknowledgment

This study was financially supported by the National Natural Foundation of China (22278279). We also thank Dr. Xiu He of the College of Biomass Science and Engineering, Sichuan University for experimental assistance.

Reference

1. Cosma, D. V., Tudoran, C., Coroș, M., et al.; Modification of cotton and leather surfaces using cold atmospheric pressure plasma and TiO_2-SiO_2-reduced graphene oxide nanopowders, *Materials* **16**, 1397, 2023.
2. Shen, Y., Zhou, J., Han, Z., et al.; Natural leather based gamma-ray shielding materials enabled by the coordination of well-dispersed Bi^{3+}/Ba^{2+} ions and RE_2O_3 coating, *Journal of Leather Science and Engineering* **4**, 15, 2022.
3. Zhu, J., Li, Z., Zou, Y., et al.; Advanced application of collagen-based biomaterials in tissue repair and restoration, *Journal of Leather Science and Engineering* **4**, 30, 2022.
4. Yu, S., Liu, H., Yang, R., et al.; Aggregation and stability of selenium nanoparticles: Complex roles of surface coating, electrolytes and natural organic matter, *Journal of Environmental Sciences* **130**, 14-23, 2023.
5. Wang, Y. N., Hu, L. Y.; Essential role of isoelectric point of skin/leather in leather processing, *Journal of Leather Science and Engineering* **4**, 25, 2022.
6. Guerrini, L., Alvarez-Puebla, R. A. and Pazos-Perez, N.; Surface modifications of nanoparticles for stability in biological fluids, *Materials* **11**, 1154, 2018.
7. Xu, Y., Fourniols, T., Labrak, Y., et al.; Surface modification of lipid-based nanoparticles, *ACS Nano* **16**, 7168-7196, 2022.
8. Hatchell, D., Song, W. and Daigle, H.; Effect of interparticle forces on the stability and droplet diameter of Pickering emulsions stabilized by PEG-coated silica nanoparticles, *Journal of Colloid and Interface Science* **626**, 824-835, 2022.
9. Wang, B., Zhong, X., Zhang, Y., et al.; Microspheres assembled by WO_{3-x} nanoparticles under action of dual surfactants: Structure and photoluminescence properties, *Optical Materials* **129**, 112550, 2022.
10. Zhao, P., Gao, D., Lyu, B., et al.; Fabrication of effective electromagnetic shielding leather with a chromium-free multi-network structure, *Journal of Cleaner Production* **374**, 133856, 2022.

11. Freitas, D. S., Teixeira, P., Pinheiro, I. B., et al.; Chitosan nano/microformulations for antimicrobial protection of leather with a potential impact in tanning industry, *Materials* **15**, 1750, 2022.
12. Ma, J., Duan, L., Lu, J., et al.; Fabrication of modified hydrogenated castor oil/GPTMS-ZnO composites and effect on UV resistance of leather, *Scientific Reports* **7**, 3742, 2017.
13. P Bhasi, A., Hanna Wilson, N. and Palanisamy, T.; Nanosized hexagonal boron nitride and polyethylene glycol-filled leathers for applications demanding high thermal insulation and impact resistance, *ACS omega* **7**, 45120-45128, 2022.
14. Elsayed, H., Hasanin, M. and Rehan, M.; Enhancement of multifunctional properties of leather surface decorated with silver nanoparticles (Ag NPs), *Journal of Molecular Structure* **1234**, 130130, 2021.
15. Pan, F., Xiao, Y., Zhang, L., et al.; Leather wastes into high-value chemicals: Keratin-based retanning agents via UV-initiated polymerization, *Journal of Cleaner Production* **383**, 135492, 2023.
16. Kumar, P., Bohidar, H.; Aqueous dispersion stability of multi-carbon nanoparticles in anionic, cationic, neutral, bile salt and pulmonary surfactant solutions, *Colloids and Surfaces A-Physicochemical and Engineering Aspects* **361**, 13-24, 2010.
17. Madshal, M. A., Abdelghany, A. M., Abdelghany, M. I., et al.; Biocompatible borate glasses doped with Gd_2O_3 for biomedical applications, *The European Physical Journal Plus* **137**, 1014, 2022.
18. Ning, G. Q., Zhou, J. B., Liao, X. P., et al.; Synthesis of a waterborne melamine resin and its retanning behaviors investigation, *JALCA* **117**, 288-295, 2022.
19. Naresh, G., Borah, J., Borgohain, C., et al.; Synthesis, characterization and effect of dopant on magnetic hyperthermic efficacy of gd2o3 nanoparticles, *Materials Research Express* **8**, 115014, 2021.
20. Peng, L. Q., Guo, L. J., Li, J. H., et al.; Rapid and highly selective removal of cesium by prussian blue analog anchored on porous collagen fibers, *Separation and Purification Technology* **307**, 122858, 2023.
21. Sun, N., Zhou, J. b., Liao, X. P., et al.; Synthesis and retanning performance of a novel melamine resin with ultralow formaldehyde content, *JALCA* **118**, 23-35, 2023.
22. Zhang, L., Chen, Y., Zhao, M., et al.; Efficient adsorption of uranyl ions from aqueous solution by Gd_2O_3 and Gd_2O_3–MgO composite materials, *International Journal of Environmental Science and Technology* **20**, 815-830, 2023.
23. Ding, W., Liu, H., Pang, X. Y., et al.; Engineering a pioneering melamine resin based on saccharide-derived aldehyde: Structure characterization and application for eco-leather production, *Industrial Crops and Products* **185**, 115133, 2022.
24. Tang, Y., Li, M. F., Zhou, J. B., et al.; Polyethyleneimine/hydrated titanium oxide-functionalized fibrous adsorbent for removing cobalt: Adsorption performance and irradiation stability, *Environmental Research* **211**, 112916, 2022.
25. Wang, G., Li, Y., Wang, E., et al.; Experimental study on preparation of nanoparticle-surfactant nanofluids and their effects on coal surface wettability, *International Journal of Mining Science and Technology* **32**, 387-397, 2022.
26. Hou, J., Du, W., Meng, F., et al.; Effective dispersion of multi-walled carbon nanotubes in aqueous solution using an ionic-gemini dispersant, *Journal of Colloid and Interface Science* **512**, 750-757, 2018.
27. Wang, X., Sun, S., Zhu, X., et al.; Application of amphoteric polymers in the process of leather post-tanning, *Journal of Leather Science and Engineering* **3**, 9, 2021.
28. Yi, Y., Zhang, Y., Mansel, B., et al.; Effect of dialdehyde carboxymethyl cellulose cross-linking on the porous structure of the collagen matrix, *Biomacromolecules* **23**, 1723-1732, 2022.
29. He, X., Huang, Y., Xiao, H., et al.; Tanning agent free leather making enabled by the dispersity of collagen fibers combined with superhydrophobic coating, *Green Chemistry* **23**, 3581-3587, 2021.
30. Li, Q., Yi, Y., Wang, Y.-n., et al.; Effect of cationic monomer structure on the aggregation behavior of amphoteric acrylic polymer around isoelectric point, *Journal of Leather Science and Engineering* **4**, 4, 2022.
31. Liu, Z., Zou, Y., Zhang, Q., et al.; Distinct binding dynamics, sites and interactions of fullerene and fullerenols with amyloid-β peptides revealed by molecular dynamics simulations, *International Journal of Molecular Sciences* **20**, 2048, 2019.

Stahl's innovations driven by sustainability

With the rise of both electric and self-driving, cars are becoming quieter and anti-squeak and rattle materials are becoming increasingly important. At the same time, improved anti-stain performance is required, because of the current trend for pale-colored car seats. Therefore, we have developed Stay Clean. This low-VOC coating technology protects pale-colored leather and vinyl surfaces against common stains, such as dye from jeans, spilled coffee and dirt. Our solution also makes surfaces low-squeak, which is a great asset as global research has shown that a squeaking car interior is one of the biggest annoyances among car owners. Another trend in car interior is the popularity of matt surfaces. Therefore, we have developed PolyMatte®. This non-squeaking solution provides a luxurious feel to the finished article in combination with flexibility and scratch and abrasion resistance. Our portfolio contains many products, varying from beamhouse products, tanning systems to finishes, duller concentrates, crosslinkers and thickeners to leveling agents, defoamers, colorants and hand modifiers. Our most sustainable option is Green PolyMatte®, which is based on rapeseed oil (20%) instead of crude oil-derived intermediates. If you would like to know what our Stahl solutions for automotive can do for your business, please visit **www.stahl.com** or contact us at: **alexander.campbell@us.stahl.com**.

If it can be imagined, it can be created

Stay Clean

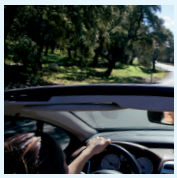

Low-VOC

PolyMatte®

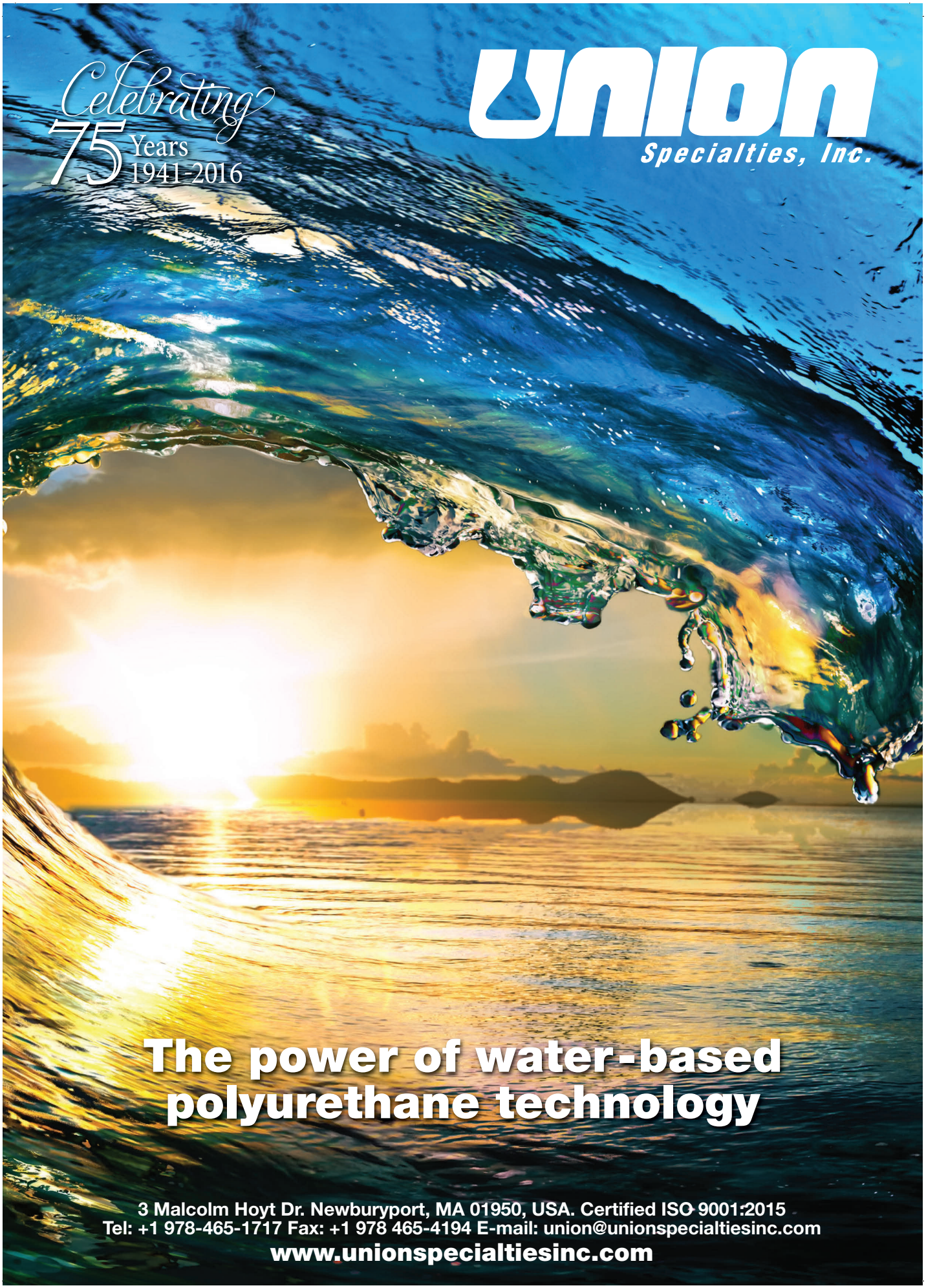
Celebrating
75 Years
1941-2016
UNION
Specialties, Inc.
The power of water-based polyurethane technology
3 Malcolm Hoyt Dr. Newburyport, MA 01950, USA. Certified ISO 9001:2015
Tel: +1 978-465-1717 Fax: +1 978 465-4194 E-mail: union@unionspecialtiesinc.com
www.unionspecialtiesinc.com

LEATHER

AVELLISYNCO

Selected Dyestuffs

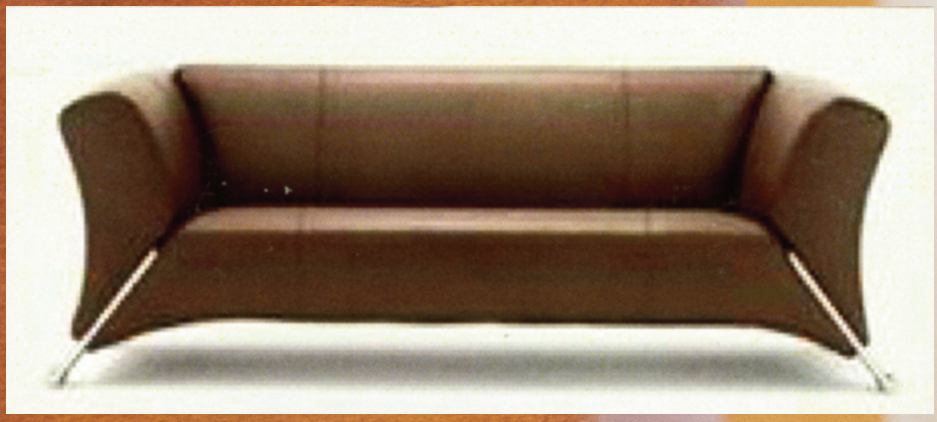

CHEMTAN

17 Noble Farm Drive • Lee, NH 03861 (Office)
57 Hampton Road • Exeter, NH 03833 (Manufacturing)
Tel: (603) 772-3741 • Fax: (603) 772-0796
www.CHEMTAN.com

Leather
is pure nature – and that feels good

We have created a polymer composed of 93% renewable materials
MAGNOPAL® Pure A is a film-forming bio-polymer and primary ingredient of the Wet-end process. It is based on vegetable biomass, a staggering 93% of which consists of renewable materials. It's free of acrylates, formaldehyde, phenol and naphthalene and is a pioneer in shifting to non-petrochemical leather manufacturing.

TFL PURE TEC PT

TFL – Great chemicals. Excellent advice.

Lifelines

Min Zhu received her Bachelor's degree in Light Chemical Engineering at Sichuan University in 2020. Now she is pursuing her Master's degree in Light Industry Technology and Engineering at Sichuan University. Her current research focuses on mass transfer and tanning effects of dialdehyde polysaccharide tanning agents.

Yudan Yi received her Master's degree in Leather Chemistry and Engineering at Sichuan University in 2020. Now she is pursuing her Ph.D. degree in Light Industry Technology and Engineering at Sichuan University. Her research interest focuses on chrome-free tanning technology.

Jia Fu is pursuing her Bachelor's degree in Light Chemical Engineering at Sichuan University. Her current research focuses on fluorescent tracing of dialdehyde polysaccharide tanning agents.

Yunhang Zeng is currently a professor in the National Engineering Laboratory for Clean Technology of Leather Manufacture, Sichuan University. She received her Ph.D. degree in Leather Chemistry and Engineering from Sichuan University in 2013. She joined Sichuan University as a lecturer from 2013 to 2016 and was an associate professor from 2016 to 2021. Her research focuses on clean leather production and leather biotechnology.

Ya-nan Wang, see *JALCA* **117**, 127, 2022.

Ting Liu is a postgraduate student at Sichuan University, China. Her research interests cover materials and chemical engineering. Her main research interest is the development and application based on protein resources. She works under the supervision of Professor Peng Biyu.

Chunxiao Zhang see *JALCA* **114**, 189, 2019.

Xu Zhang see *JALCA* **117(10)**, 2022.

Biyu Peng see *JALCA* **117(10)**, 2022.

Mengchu Gao see JALCA **117(10)**, 2022.

Song Guo: Guo Song earned his BE degree in Light Chemical Engineering from Sichuan University (2011). He received his MS degree (2014) in Leather Chemistry and Engineering from Sichuan University. He then joined the faculty of China Leather and Footwear Research Institute Co. Ltd. in 2014. His interests include leather science, nano materials and collagen-based materials.

Wei Ding: Wei Ding earned his BE degree in Light Chemical Engineering from Sichuan University (2010). He received his MS degree (2013) and PhD (2016) in Leather Chemistry and Engineering from Sichuan University. He then became a postdoctoral fellow at Guangdong Dymatic Fine Chemicals Inc. He joined the faculty of China Leather and Footwear Research Institute Co. Ltd. in 2019. His interests include leather science, biomass conversion, collagen-based materials and advanced coating materials.

Xiaoyan Pang: Xiaoyan Pang earned her bachelor's degree in leather engineering (2002) and received her master's degree in applied chemistry from Shaanxi University of Science and Technology (2005). In 2019, she received a PhD degree in biomass chemistry and engineering from Sichuan University. In 2005, she joined China Leather and Footwear Research Institute Co., LTD. Her interests include leather science and biomass-based functional materials.

Zhiwen Ding: Ding Zhiwen graduated from Sichuan University and received his PhD degree in 2001, He is the deputy president of China Leather and Footwear Industry Research Institute. His interests include clean leather making technologies, utilization technologies of leather waste, and collagen-based materials.

Jibo Zhou received his master's degree in Biomass Chemistry and Engineering from Sichuan University in 2019. He is currently pursuing his doctoral program in Biomass Chemistry and Engineering under the supervision of Prof. Xuepin Liao in Department of Biomass and Leather Engineering, Sichuan University, China. His research interests include leather chemicals and functional leather products.

Nan Sun, see *JALCA* **118**, 23, 2023.

Xuepin Liao, see *JALCA* **113**, 198, 2018.

Bi Shi, see *JALCA* **99**, 220, 2004.

WARDROBE MALFUNCTION

LEATHER. IF WE DON'T USE IT, WE DO MORE THAN JUST LOSE IT.

From food to fashion, a burger and shake is just the start of the story of waste and recklessness. We live in a world where the cheap and easy option is to throw away the byproducts of our society. Instead we crop new land, drill or frack for short lived replacements. Isn't it time to shake things up, to think slow instead of fast. To think of our future and that of the planet?

300M HIDES COME FROM THE MEAT & DAIRY INDUSTRIES EVERY YEAR

60% IS USED FOR LEATHER. THE REST IS JUST TROWN AWAY

THAT IS **120M** 3M TONNES OF LANDFILL & 2.7M TONNES OF GREENHOUSE GASES. EVERY YEAR.

THE FASHION INDUSTRY PRODUCES

144 BILLION ITEMS OF CLOTHING EVERY YEAR

WE NEED 3.5M ACRES OF FOREST, JUST TO RE-CAPTURE THE CARBON CREATED BY THIS WASTE.

65% OF ALL OUR CLOTHES ARE PLASTIC, SOURCED THROUGH DRILLING & FRACKING

EACH HIDE COVERS **4 SQM**

WE WASTE NEARLY **480 MILLION SQM**

OF MATERIAL EACH YEAR, ENOUGH TO COVER

78,000 FOOTBALL PITCHES

OR TO PUT SHOES ON THE FEET OF

EVERY MAN, WOMAN & CHILD IN AFRICA

AND ONE LEATHER ITEM CAN LAST A LIFETIME

TO JOIN THE DISCUSSION FIND US AT: CHOOSEREALLEATHER.COM

Sometimes Safety Begins with Reflection

Chemtan®
Reflect V-100

CHEMTAN

Tel: (603) 772-3741 • www.CHEMTAN.com